

Impact of natural (waves and currents) and anthropogenic (trawl) resuspension on the export of particulate matter to the open ocean Application to the Gulf of Lion (NW Mediterranean)

B. Ferré^a, X. Durrieu de Madron^{a,*}, C. Estournel^b, C. Ulses^b and G. Le Corre^c

^a CEFREM, CNRS—Université de Perpignan, Perpignan, France

^b LA, CNRS—Université de Toulouse, Toulouse, France

^c IFREMER, DRH, Sète, France

*: Corresponding author : X. Durrieu de Madron, Tel.: +33 4 68 66 22 48; fax: +33 4 68 66 20 96, email address : demadron@univ-perp.fr

Abstract:

Modern sediment deposits on continental margins form a vast reservoir of particulate matter that is regularly affected by resuspension processes. Resuspension by bottom trawling on shelves with strong fishing activity can modify the scale of natural disturbance by waves and currents. Recent field data show that the impact of bottom trawls on fine sediment resuspension per unit surface is comparable with that of the largest storms.

We assessed the impact of both natural and anthropogenic processes on the dispersal of riverborne particles and shelf sediments on the Gulf of Lion shelf. We performed realistic numerical simulations of resuspension and transport forced by currents and waves or by a fleet of bottom trawlers. Simulations were conducted for a 16-month period (January 1998–April 1999) to characterise the seasonal variability. The sediment dynamics takes into account bed armoring, ripple geometry and the cohesive and non-cohesive characteristics of the sediments. Essential but uncertain parameters (clay content, erosion fluxes and critical shear stress for cohesive sediment) were set with existing data. Resuspension by waves and currents was controlled by shear stress, whereas resuspension by trawls was controlled by density and distribution of the bottom trawler fleet.

Natural resuspension by waves and currents mostly occurred during short seasonal episodes, and was concentrated on the inner shelf. Trawling-induced resuspension, in contrast, occurred regularly throughout the year and was concentrated on the outer shelf. The total annual erosion by trawls ($5.6 \times 10^6 \text{ t y}^{-1}$, t for metric tonnes) was four orders of magnitude lower than the erosion induced by waves and currents ($35.3 \times 10^9 \text{ t y}^{-1}$). However the net resuspension (erosion/deposition budget) for trawling ($0.4 \times 10^6 \text{ t y}^{-1}$) was only one order of magnitude lower than that for waves and currents ($9.2 \times 10^6 \text{ t y}^{-1}$).

Off-shelf export concerned the finest fraction of the sediment (clays and fine silts) and took place primarily at the southwestern end of the Gulf. Off-shelf transport was favoured during the winter 1999 by a very intense episode of dense shelf water cascading. Export of sediment resuspended by trawls ($0.4 \times 10^6 \text{ t y}^{-1}$) was one order of magnitude lower than export associated with natural resuspension ($8.5 \times 10^6 \text{ t y}^{-1}$). Trawling-induced resuspension is thought to represent one-third of the total export of suspended sediment from the shelf.

A simulation combining both resuspension processes reveals no significant changes in resuspension and export rates compared with the sum of each individual process, suggesting the absence of interference between both processes.

Keywords: Sediment dynamics; Sediment transport; Shelf–slope exchanges; Fisheries; Trawling; Mediterranean

34 **1. INTRODUCTION**

35 Continental margins are located at the edges of continents and form a buffer zone where the oceans,
36 continents and atmosphere interact. Significant quantities of organic and inorganic material are input
37 to continental margins where intense hydrodynamic conditions control their dispersal on the shelf and
38 towards the open sea. The sedimentary compartment on continental margins appears to be a vast
39 reservoir of particulate matter, in particular river-derived material, and also of dissolved elements.
40 Resuspension of sediment causes a significant redistribution of sediments and has important
41 implication for regional particulate matter budgets and export to deeper environments, i.e. the
42 continental slope and rise.

43
44 Nowadays the physical resuspension and disturbance of sediment on continental shelves is a
45 combination of both natural and anthropogenic mechanisms. Waves and currents are the major
46 initiators of natural disturbance that can result in potentially massive sediment redistribution. The
47 large-scale disturbance they induce can be periodic, when associated with tidal currents, or episodic,
48 when associated with storms. On the other hand, commercial bottom trawling has a more reduced and
49 patchy print. Bottom fishing gears (trawl, dredge) efficiently scrap the superficial sediment and
50 generate suspended sediment plumes. In many shelves fishing intensity is high and most fishable
51 grounds, which can extend to 1000 m in depth, are likely to be disturbed more or less frequently. The
52 effect of sediment resuspension by waves and currents and bottom trawling is site-specific, as it
53 depends on hydrodynamic conditions (storm frequency and intensity, tidal motions), sediment
54 characteristics (grain size, cohesiveness), and fishing activity (frequency and geographical distribution
55 of bottom hauls, gear type).

56
57 The relative contribution of each mechanism to the resuspension and export of sediment on
58 continental shelves has seldom been addressed. To our knowledge, Churchill (1989) and DeAlteris *et*
59 *al.* (1999) carried out the only preliminary studies on the comparison of the effect of natural and
60 anthropogenic resuspension on different areas of the Mid-Atlantic Bight (Narraganset Bay, Nantucket
61 Shoals, and Virginia Shelf). These studies concluded that natural physical processes are the primary
62 suspension mechanism in shallow environments, where they disturb the bed regularly, while trawling
63 appears to be the primary resuspension mechanism in deeper environments where natural processes
64 are weaker and rarely capable to erode sediment. Furthermore, Churchill (1989) estimated, using
65 current meter data and simple analytical models, that transport of sediment resuspended by trawlers
66 on muddy regions of the outer shelf could contribute to the off-shelf transport of particulate matter.

67
68 The present paper aims to assess the impact of sediment resuspension on particulate matter budgets
69 on the Gulf of Lion continental shelf (NW Mediterranean). It discriminates the impact of natural
70 physical (waves and currents) and anthropogenic (bottom trawling) processes, and thereby check
71 whether anthropogenic disturbance represents a significant or just a slight modification in the scale of
72 existing natural disturbance. This work uses three-dimensional numerical models coupling the

73 hydrodynamics with the sediment dynamics, associated with waves and currents and/or trawling. The
74 characteristics of the models are based on experimental studies of the resuspension of fine sediments
75 by intense storms (Ferré *et al.*, 2005; Ulses *et al.*, submitted) and trawls (Durrieu de Madron *et al.*,
76 2005). Simulations over one annual period, using realistic forcings, were carried out to characterise
77 and quantify (i) the temporal variability and magnitude of sediment resuspension on the shelf, (ii) the
78 dispersal of resuspended sediment, and (iii) the export towards the open sea.

79

80 The outline of this paper is as follow: the regional setting is described in section 2, the hydrodynamical
81 and sediment transport models are briefly described in section 3, the numerical simulations of
82 sediment resuspension and export are exposed in section 4, comparison of resuspension processes
83 and their impact of the sediment budgets are presented in section 5, a summary is given in section 6,
84 and the model equations are given in the appendix.

85

86

87 **2. REGIONAL SETTING**

88 **2.1 Physiography and hydrodynamics**

89 The Gulf of Lion is a non-tidal and river-dominated margin in the northwestern Mediterranean (Fig.
90 1a). It is fed by ten rivers, one of them being the Rhône, which is the major Mediterranean river. Its
91 crescent shape and the circulation patterns favour off-shelf export of particulate matter at the
92 southwestern end of the Gulf (Monaco *et al.*, 1999; Heussner *et al.*, 2006, Palanques *et al.*, 2006).

93 The grain size distribution of superficial bottom sediments is shown in Fig. 1b. Sands of the inner shelf
94 display a seaward-fining texture and merge with mid-shelf muds in water deeper than 20–30 m. The
95 only noticeable exception is the prodeltaic accumulation zones found near river mouths, which are
96 composed of silty muds. Muddy deposits on the outer shelf (>90 m) are mixed with relict sandy
97 outcrops.

98 The different wind regimes determine the natural resuspension and transport of suspended sediment
99 on the shelf. N-NW winds induced distinctive and opposite circulation cells on the shelf, favouring
100 intrusion of slope waters in the eastern and central parts, and export of shelf water at the
101 southwestern end of the Gulf (Estournel *et al.*, 2003; Petrenko *et al.*, 2004). Furthermore, these cold
102 and dry continental winds are responsible for the strong cooling and homogenisation of the shelf water
103 column during winter, and eventually generate dense water (Dufau-Julliard *et al.*, 2004; Ulses *et al.*,
104 accepted). Due to the reduced fetch, N-NW winds generate small waves (significant wave height
105 < 2 m, peak period < 6 s) on the inner shelf. Conversely, E-SE winds are episodic and short-lived, but
106 are associated with a long fetch and large swell (significant wave height up to 10 m, peak period up to
107 12 s). River floods often occur in conjunction with E-SE storms as the transport of humid marine air
108 over coastal relief induces abundant precipitations. Resuspension by natural physical processes

109 results primarily from the effect of southeasterly swells associated with E-SE winds (Ferré *et al.*, 2005,
110 Guillén *et al.*, 2006).

111 A permanent cyclonic current (the Northern Current) flows along the slope and is part of the general
112 circulation of the western Mediterranean basin (Millot, 1999). It forms a density front that separates the
113 low-salinity shelf water from the more saline open sea water, limiting the off-shelf dispersal while
114 enhancing along-slope dispersal (Durrieu de Madron *et al.*, 1990; Lapouyade and Durrieu de Madron,
115 2001).

116

117 **2.2 Characteristics of trawling activity**

118 About 128 trawlers coming from the local fishing ports (Port-Vendres, Port-la-Nouvelle, Agde, Sète,
119 Grau du Roi, Port de Bouc) are working in the Gulf of Lion, using either semi-pelagic or bottom trawls
120 to catch demersal fish species. Bottom trawler use single trawl nets tightened between doors (otter)
121 with a tickler chain as a groundrope. Pelagic trawls are sometimes also used very near the seabed,
122 but Durrieu de Madron *et al.* (2005) showed that they had no impact on the sediment resuspension.
123 The daily number of trawlers using bottom trawls ranges approximately between 40 and 90 boats,
124 each trawler performing 4 to 5 tows of about 2 hours daily. They work throughout the year except
125 weekends and public holidays.

126 Fishing grounds cover the whole continental shelf except a 3-miles coastal band, where all trawling
127 activity is banned. A survey conducted with fishermen revealed that the wind is the principal criterion
128 for the choice of the fishing grounds. Trawlers remain basically close to the coast during strong winds
129 ($> 10 \text{ m s}^{-1}$ or 20 knots) and rough seas state periods, and move to the outer shelf for weaker winds
130 and calmer sea state (Fig. 2).

131

132 **3. MATERIAL AND METHODS**

133 **3.1 Hydrodynamical model**

134 *The SYMPHONIE Model* - The three-dimensional primitive equation coastal ocean model
135 SYMPHONIE, used in this study, has been extensively validated in the Gulf of Lion. It was previously
136 used to study the Rhône river plume (Estournel *et al.*, 1997; Marsaleix *et al.*, 1998; Estournel *et al.*,
137 2001), the intrusion of the Northern Current into the shelf (Petrenko *et al.*, 2004), the wind-induced
138 circulation (Estournel *et al.*, 2003) and the formation of dense water on the shelf and its cascading
139 over the slope (Dufau-Julliand *et al.*, 2004; Ulses *et al.*, accepted).

140

141 The three current components, free surface elevation, temperature and salinity are computed on a C
142 staggered-grid (Arakawa and Suarez, 1983). A generalized topography following co-ordinate system is
143 used. Compared to simple sigma coordinate, the generalized sigma coordinate allows the slope of the
144 iso-level surface to be limited over steep topography in order to avoid large truncation errors on the
145 pressure gradient computation (Auclair *et al.*, 2000). The turbulence closure scheme is based on a
146 prognostic equation for the turbulent kinetic energy and on a diagnostic equation for the mixing and
147 dissipation length scales (Bougeault and Lacarrère, 1989). A leap frog scheme is used for the time-
148 stepping. A time-splitting technique (Blumberg and Mellor, 1987) allows the vertical shear of the
149 current and the depth-averaged horizontal components to be computed separately with appropriate
150 time steps.

151

152 *Initialisation and boundary conditions* - The domain of the Gulf of Lion model (25 vertical levels and 3
153 km horizontal resolution grid) is presented in Figure 1a. The main boundary of the modelling domain
154 has been chosen to be parallel to the continental slope.

155

156 At the surface, the momentum flux is equal to the wind stress. The heat flux results from the
157 atmospheric fluxes (sensible and latent heat fluxes) and from the radiative fluxes (both short and long
158 wavelengths), the salinity flux is calculated from evaporation. Concerning the flux of turbulent kinetic
159 energy, the usual boundary-layer balance between production and dissipation is applied. The wind
160 stress and the heat fluxes are computed with the bulk formulae (Geernaert, 1990) using 6-hours
161 outputs of the high resolution meteorological models ARPEGE and ALADIN from Météo-France
162 (surface pressure, air temperature, relative humidity and wind velocity) and the sea surface
163 temperature is computed by the ocean model.

164

165 At the sea floor, the near-bottom stress is related to the horizontal bottom velocity and waves, as well
166 as the seabed roughness. A detailed description of this term is given in appendix 2. Heat and salinity
167 fluxes are considered to be zero at this boundary. The flux of turbulent kinetic energy is parameterised
168 similarly as the one at the surface boundary.

169

170 At open lateral boundaries, the free-surface elevation (η) and the component of transport orthogonal to
171 the boundary (U) are given by the radiation condition of Oey and Chen (1992): $U=U_0 \pm (gH)^{1/2} (\eta-\eta_0)$.
172 Others variables are given by $\nabla_H \varphi = \nabla_H \varphi_0$, where φ stands for the tangential component of the depth
173 averaged current and baroclinic velocities. U_0 , φ_0 and η_0 refer to the large scale field forcing.
174 Concerning temperature and salinity, an upstream condition implies that large-scale fields, $T_0(t)$ and
175 $S_0(t)$, are advected into the simulated domain under inflow conditions. The large-scale fields are also
176 applied over the whole grid at $t=t_0$ (initialisation). This initial state aims to start the simulation with the
177 large-scale geostrophic circulation of the Gulf of Lion, generally identified as the Northern Current. The
178 model is initialised with a fully established along slope circulation adjusted to bathymetry constraints,
179 based on a linearised derivation of the external mode equations of the model (Estournel *et al.*, 2003).

180 The regional model was initialized and forced every day by the large scale Ocean General Circulation
181 Model (OGCM) MOM outputs. Wave characteristics over the domain were described by the 6-hour
182 outputs of the Vagmed waves-forecast model of Météo-France.

183
184 Concerning the buoyancy inputs, the freshwater inputs for the main rivers of the Gulf of Lion (Grand-
185 Rhone, Petit-Rhone, Vidourle, Lez, Herault, Orb, Aude, Agly, Têt, Tech) (see Fig. 1a), are taken into
186 account. Daily discharges provided by the 'Compagnie Nationale du Rhône' and by the 'Banque
187 Hydro-MEDD/DE' were specified at the ten river mouths. The temperature in all rivers is set following
188 measurements in Rhone river (Poirel *et al.*, 2001), with a maximum value of 22 °C in October and a
189 minimum value of 7 °C in January and February.

190

191 **3.2 Sediment transport model**

192 The suspended sediment transport model aims at simulating the dispersal of the sedimentary particles
193 resuspended by waves and currents, as well as bottom trawls. This model is governed by an
194 advection-diffusion dispersion equation, and considered different particle grain sizes (see appendix 1).
195 Deposition and erosion terms are incorporated into the seabed boundary condition. The erosion term
196 was estimated with sediment dynamic models specific to each resuspension mechanisms (waves and
197 current, trawl); they are described in the following chapters and in appendix 2.

198 Given that the Gulf of Lion sediments cover a wide range of size (Fig. 1b), primary (individual) particles
199 in the sediment were clustered in 7 size classes ranging from clay to coarse sand, according to the
200 Wentworth classification (1922). Two additional classes were considered for suspended particles to
201 take into account aggregated particles. The aggregates characteristics were inferred from
202 comparisons between *in situ* and laboratory particle size distribution of resuspended sediment (Durrieu
203 de Madron *et al.*, 2005). These measurements suggested that about $\frac{3}{4}$ of the clays and $\frac{1}{4}$ of the fine
204 silts are incorporated into aggregates whereas the rest remains as primary particles. We considered
205 that clays and fine silts contributed equally to the formation of both classes of aggregates. The
206 characteristics of each class (median grain size, settling velocity and density) are indicated in the
207 Table 1.

208 River sediment inputs were computed using water discharge (Q) and suspended sediment
209 concentration estimates ($SSC=f(Q)$) established by different authors: Sempéré *et al.* (2000) for the
210 Rhône River, Petelet-Giraud *et al.* (2003) for the Herault River, Serrat (1999) for the Agly River, and
211 Serrat *et al.* (2001) for the Têt River. In absence of information for Orb and Aude Rivers, we used the
212 relationship of the nearby Herault River. Finally, solid discharge of the Rhône River was divided into
213 two parts: 90% for the Grand-Rhône branch and 10% for the Petit-Rhône branch. Grain size
214 distribution of river inputs was defined according to recent data collected in the Rhône River
215 (Radakovitch, personal communication) and Têt River (Garcia-Esteves, 2005). All "small" rivers
216 (Hérault, Agly, Orb, Aude, Vidourle and Tech) are considered to have the same grain distribution than

217 the Têt River. Most of the suspended particles are silts (ca 80% for the Rhône River and 69% for the
218 Têt River) and clays (~ 18% for the Rhône River and 24% for the Têt River).

219 The grain size distribution of the shelf surface sediments was determined from the compilation of
220 several sedimentological surveys that provided about 160 cores over the whole shelf. Figure 1b shows
221 the median grain size of the first centimetres of the sediment. Maps of the fraction of the different size
222 classes were used at the initial time. Their characteristics slightly changed throughout the simulation
223 according to the dispersal of river inputs, and the erosion and deposition of the different classes of
224 sediment.

225 **3.3 Sediment dynamics for waves and currents**

226 The sediment erodability is controlled by the shear stress intensity and the bottom sediment properties
227 (coarse non-cohesive vs. fine cohesive sediments). The limit between cohesive and non-cohesive
228 sediment was fixed at 10 % of clay (<2 μm), which is in the range (3-14%) defined in various studies
229 (Dyer, 1986; Torfs, 1995; Panagiopoulos *et al.*, 1997; Houwing, 2000). The Partheniades' law (1962)
230 was used to compute the erosion flux of cohesive sediments, whereas the reference concentration
231 based on the method of Zyserman and Fredsøe (1994) was used for the erosion flux of the non-
232 cohesive sediments (see appendix 2).

233 The stress values were computed using combined wave and currents conditions, and discriminated
234 flat-bed and rippled bed conditions (see appendix 2). The bottom roughness calculation and ripples
235 geometry for the non-cohesive sediments was based on the SEDTRANS96 model (Li and Amos,
236 1998; Li and Amos, 2001), which predicts the roughness and bedforms generated by a combined
237 wave/current model. For cohesive and mixed sediments, the roughness scale model of Harris and
238 Wiberg (2001) was used. Besides, bed armoring was implemented in the model to take into account
239 the reduction of erosion flux of fine particles in mixed sediments, due to the protective effect of larger
240 sand grains (Harris and Wiberg, 2001).

241 The critical shear stress (stress above which the sediment is likely to be removed) depends on grain
242 size and sediment characteristics. For non-cohesive sediments, the critical shear stress is given in the
243 form of a critical Shields parameter value, which depends on the grain size of each class (see
244 appendix 2). For cohesive sediments, the threshold value is difficult to establish because it depends
245 on the compaction and history of the sediment. Indeed, unconsolidated surface layer (fluff) is eroded
246 for very weak shear stresses, ranging between 0.02 and 0.08 N m^{-2} (El Ganaoui *et al.*, 2004; Gust and
247 Morris, 1989; Maa *et al.*, 1998; Schaaff *et al.*, 2002). The underlying, more consolidated layers, need
248 larger critical shear stresses, between 0.1 and 0.61 N m^{-2} (Maa *et al.*, 1998; Houwing, 1999;
249 Krishnappan and Marsalek, 2002, Palanques *et al.*, 2002). In this study we considered an average
250 critical shear stress of 0.2 N m^{-2} .

251

252 **3.4 Resuspension by bottom trawls**

253 In absence of direct information of distribution and movement of trawler on the shelf, we used a
254 probabilistic approach to simulate their position and trajectory. The daily schedule and number of
255 active bottom trawlers was estimated from records of trawler fleet coming from different fishing ports
256 (Fig. 3d). During working days, each trawler was assumed to perform 4 tows of 2 hours from 4 a.m. to
257 12 a.m.

258 A probabilistic distribution of fishing effort was simulated for both wind conditions, using several
259 variables (depth, distance from the ports to the different fishing areas, and fishing rules in force in the
260 area) (Fig. 2). The distribution map for each working day was selected according to the wind intensity
261 next to the Sète port (major fishing port of the area) at 4 a.m. After being positioned randomly, each
262 trawl was displaced using a random walk approach. Given the mesh size of the model (3 km) and the
263 trawling speed (1.5 m s^{-1}), a crossing time of 33 min was considered before moving each trawler to
264 one of the surrounding mesh. A maximum number of 3 trawlers per mesh was imposed.

265 The fluxes of sediment resuspended by otter bottom trawls and the characteristics of the sediment
266 plumes were estimated by Durrieu de Madron *et al.* (2005). They showed that resuspension fluxes
267 depend on the trawls groundrope gears, and above all on sediment texture (i.e., clay content) (see
268 appendix 2). According to observations, resuspended sediment was distributed over the last 5 m
269 above the seabed with a concentration inversely proportional to the seabed distance. For each time
270 step (180 s), the resuspended mass of sediment is proportional to the trawled area: 4320 m^2
271 considering a trawler speed of 1.5 m s^{-1} , and a combined net and door width of 16 m. Because this
272 area is much smaller than that of the model's mesh (9 km^2), the resuspended mass was spread over
273 the entire mesh and within layers including the last 5 m above bottom. The bias introduced by the
274 forced diffusion is likely to be small, since most of the resuspended sediment is rapidly deposited
275 (within 1-2 hours according to Durrieu de Madron *et al.*, 2005), and remains confined to the adjacent
276 meshes.

277 **3.5 Scenarios and numerical solutions**

278 Four scenarios were carried out in order to answer the question about the role of resuspension in the
279 shelf-slope exchanges of particulate matter. They considered the same hydrodynamic forcings
280 described in chapter 3.1.

- 281 - The first simulation, which only takes into account the river particulate inputs, (i.e. resuspension is
282 absent), was used as reference for the shelf deposit and the export of riverine particulate matter
283 for the study period;
- 284 - The second scenario considered, in addition to the preceding simulation, resuspension of
285 sediment by currents and waves only;

- 286 - The third scenario considered the sediment resuspension by trawls only;
- 287 - A fourth scenario combining resuspension by waves and currents, as well as trawls, checked if
- 288 there is any significant non linear effect.

289 Simulations lasted 16 months from January 1, 1998 to April 1, 1999. The water column was clear of
290 suspended particles at the initial time, and the system was gradually loaded in suspended particles,
291 coming from rivers and/or sediment resuspension during the first months of simulations. As the
292 residence time of shelf waters is about 2 months (Durrieu de Madron *et al.*, 2003), we checked that the
293 suspended sediment concentration (SSC) of the shelf water was stabilized on the third month (March
294 1998). For each scenario, annual budgets of resuspended sediment, deposited particles on the shelf,
295 and exported particles to the slope, were calculated between April 1998 and April 1999.

296 Hydrology and circulation on the shelf and upper slope were measured for two surveys conducted in
297 March/April 1998 and January 1999. Previous studies tested the ability of the hydrodynamical model
298 to correctly reproduce the hydrology and the wind-induced circulation patterns observed in March/April
299 1998 (Estournel *et al.*, 2003), and the formation of dense water on the shelf and its cascading over the
300 slope in January/February 1999 (Dufau-Julliand *et al.*, 2004). Critical but indefinite parameters of the
301 sediment dynamics model (i.e., clay content threshold for cohesive/non-cohesive behaviour, erosion
302 flux and critical shear stress for cohesive sediments) were adjusted to fit the *in situ* observations (47
303 casts) collected all over the shelf during these surveys (Fig. 1a). The agreement was quantified by
304 computing the differences between simulated SSC values (combining both resuspension by waves
305 and current conditions and trawling activity) within the last three levels above the bottom with observed
306 near-bottom SSC, estimated from optical (light transmission) measurements. The adjusted parameters
307 yielded differences in SSC less than 35% for more than half of the stations and maximum differences
308 of 80%.

309 4. RESULTS

310 Hydrodynamical conditions.

311 During the simulation period (April 1998 – April 1999) the Rhône River supplied respectively 80% of
312 the freshwater and 90% of the suspended sediment inputs to the Gulf (Fig. 3a). The annual total solid
313 discharges amounted to 3.6×10^6 T, that were supplied during medium floods occurring mostly during
314 the spring 1998 and late autumn 1998-winter 1999 (Fig. 3b). Given that the average sediment
315 discharge from the Rhône over the 1977-2004 period is about 10.1×10^6 T y⁻¹ and peaks at more than
316 33×10^6 T y⁻¹ (Bourrin *et al.*, 2007), the 1998-1999 period appears as a low discharge year.

317 E-SE gales were rare and brief but caused locally strong precipitations and sudden floods. N-NE
318 continental winds were predominant throughout the year (Fig. 3c). These cold and dry winds affected
319 the annual cycle of the shelf water thermal characteristics, by inducing strong mixing and cooling

Formatted: Bullets and Numbering

320 during fall and winter. As the average salinity of the shelf water was rather constant all over the year,
321 decreasing temperature induced a progressive increase of density that culminated in late winter (Fig.
322 3f). During winter and early spring, large quantities of dense shelf water overflowed the shelf break
323 and cascaded down the slope (Fig. 3g), especially in February/March 1999. Export of water mainly
324 occurred in the western part of the shelf, and was compensated by an inflow in the eastern part of the
325 Gulf. Béthoux *et al.* (2002) showed that an event of such intensity had not occurred since 1993, and
326 that the last event probably went back to the winters 1987-1988. An event of similar intensity was
327 observed in winter 2005 (Canals *et al.*, 2006).

328 Bottom stress presents a seasonal cycle with larger values between the end of autumn and the
329 beginning of spring (Fig. 3e), due to the increase of the current intensity and wave conditions, and also
330 to the weak stratification of the water column. Wind intensity and direction variability induced many
331 bursts in the bottom stress, which was generally more intense on the western part of the shelf.

332 In summary, the study period was characterized by low river discharges and moderate wave
333 conditions (with few E-SE storms), but by intense winter shelf water export through dense water
334 cascading caused by sustained N-NW winds.

335

Formatted: Bullets and Numbering

336 **Fate of river inputs without resuspension.**

337 A first simulation was carried out by taking into account the sediment supplied by rivers only, in order
338 to estimate the direct contribution of rivers to the sediment export (Fig. 4). During the April 1998 - April
339 1999 period 3.6×10^6 T of sediment were discharge by rivers (Table 2). As previously mentioned, most
340 of inputs derived from the Rhône River. Deposits of river sediment on the shelf, which amount to
341 3.1×10^6 T, clearly reflect the difference in river discharges (Fig. 3a). Sediments supplied by the
342 Hérault, Orb, and Aude Rivers in the northwestern part of the Gulf remained primarily confined to the
343 inner shelf. Deposit of the Rhône River inputs formed a wedge extending over the eastern part of the
344 shelf and the outer shelf as far as the southwestern end of the Gulf. The net deposit thickness was
345 largest near the major river mouth, and was about 0.1 mm on most of the shelf. The grain size
346 distribution reflected the accumulation gradient, with an early settling of the coarser particles on the
347 prodeltas, and a fining texture along the transport pathways. Sediments in suspension exported from
348 the shelf were mainly composed of fine particles. The exported quantity was 0.4×10^6 T (only 11% of
349 river inputs (Table 2) and occurred for the two thirds during wintertime (Dec. 1998 – Apr. 1999).

350

Formatted: Bullets and Numbering

351 **Dynamics of resuspended sediments**

352 *Resuspension and off-shelf sediment export induced by waves and currents* – Time series of the daily
353 mass of sediment resuspended on the shelf (Fig. 5a) showed that resuspension by waves and

354 currents appeared as short events, with a maximum duration of a few days, throughout the year.
355 Some larger and longer resuspension events were to be noted in spring and fall 1998, and also during
356 December 1998 and February 1999, due to the action of stronger coastal currents or swells. During
357 the April 1998 - April 1999 period about 35.3×10^9 T of sediment were resuspended (Table 2),
358 preferentially on the inner shelf (water depth < 50 m (Fig. 6), and the largest part was composed of
359 coarse sediments that quickly settled. The annual net erosion/deposition budget amounted to
360 9.2×10^6 T (Table 2), which was more than twice the annual river inputs.

361 Off-shelf export occurred as bursts, which immediately followed the resuspension events. They were
362 generally of short duration except for a sustained period in February and March 1999 due to dense
363 shelf water cascading (Fig. 5b and 13). Water flux at the shelf break (Fig. 3g) indicated that the two
364 summer pulses on mid-June and mid-September 1998 occurred on the eastern part of the Gulf, while
365 that all the other episodes occurred in its western part. The annual export of sediment solely
366 resuspended by waves and currents amounted to 8.5×10^6 T (Fig. 13), which represented about 0.02%
367 of the resuspended quantity (Table 2). The exported sediment was mostly composed of clays and fine
368 silts, but the strong cascading-driven currents induced an export of larger particles (including sands)
369 during the winter 1999.

370 The map of erosion and deposition regions at the end of the annual cycle (Fig. 6) indicated a net
371 deposit over most of the shelf, except within the coastal band shallower than 30 m, and also on the
372 southwestern outer shelf. Resuspension by waves and currents induced a total redistribution of the
373 riverine sediments, but did not significantly change the initial grain size distribution of the shelf
374 sediments (i.e., cross-shelf gradient with coarser sediment near the coast and finer sediment
375 seaward). Regions of stronger deposit were localised along a band between 30 and 70 m deep,
376 extending from the Rhône River as far as Cape of Creus, which constitutes a natural outlet at the
377 southwestern end of the Gulf. This band, which mimics the mid-shelf mud belt, was primarily
378 composed of fine particles. Erosion of sediment by waves and currents was observed in the head of
379 the westernmost canyons during the winter cascading period.

380
381 The dispersal of suspended sediment on the slope was variable according to the period of the year.
382 From May to November, while the water column was stratified, the export of shelf suspended sediment
383 was primarily restricted to the surface slope waters (Fig. 7a). The seaward dispersal in the upper layer
384 (0-500m) was limited by the core of the permanent cyclonic Northern Current that swept, along the
385 slope, the material escaping from the shelf. From December to April, whilst the water column was
386 weakly stratified or even unstable during the dense water cascading period, shelf suspended sediment
387 rapidly spread into intermediate (500-1000 m) or deep (> 1000 m) slope waters (Fig. 7b).

388
389 *Resuspension and off-shelf sediment export induced by trawls* - Conversely to the natural
390 resuspension which occurs as irregular and short episodes, bottom trawling activity is periodic and
391 rather constant over the whole year (Fig. 3d). Resuspension by trawls is dependant on the trawl
392 number and positions. During the April 1998 - April 1999 period, bottom trawlers worked 250 days and

393 the fishing fleet had a daily mean strength of 63 boats. The total surface scraped by trawlers during
394 this annual period amounted to 11,000 km², which is comparable to the surface of the Gulf of Lion
395 shelf (ca 12,000 km²). Some regions were trawled several times a year, whereas others were
396 untouched. For strong winds (> 10 m s⁻¹), trawlers were mostly confined to the coastal area, where
397 coarse sediment is more abundant (Fig. 2a). Days of strong winds were present 13% of the year, most
398 of the time in autumn and winter. During low wind periods (≤ 10 m s⁻¹), trawlers preferentially worked
399 on the outer shelf and eroded finer sediment (Fig. 2b). About 2.2×10⁴ T of sediment were resuspended
400 daily by bottom trawls (Fig. 8a), with a maximum between September and December 1998 when
401 trawlers were more numerous (> 80, Fig. 3d). The annual mass of sediment resuspended by trawling
402 amounted to 5.6×10⁶ T (Table 2), most of it originating from depths between 80 and 130 m (Fig. 9).
403 Considering the fraction that settled shortly after resuspension, the annual net erosion/deposition
404 budget on the shelf amounted to 0.4×10⁶ T (Table 2), which was one order of magnitude less than that
405 induced by waves- and current-induced resuspension.

406
407 The export of resuspended sediment from the shelf showed a seasonal variability, with minimum
408 fluxes during summertime (whilst the resuspension on shelf was maximum), and a significant increase
409 arising from transport pulses during the winter and spring periods. The fine-grained sediment
410 resuspended by trawlers on the outer shelf was exported primarily in the western half of the Gulf (Fig.
411 9). The off-shelf export added up to 0.4×10⁶ T annually, which accounted for ~7% of the quantity of
412 sediment resuspended by trawling on the shelf (Table 2 and Fig. 13).

413 Transects showed that the cross-slope dispersal of the fine-grained sediment resuspended by trawlers
414 went deeper than for the sediment resuspended by waves and currents, due probably to the proximity
415 of regions of intense trawling activity with the shelf edge. Some sediment reached by settling depths of
416 1500-2000 m during summer stratified condition (Fig. 10a). Cascading of dense water during winter
417 caused a rapid advection of turbid shelf water down to 1000 m deep, and settling favoured the
418 spreading of suspended sediment as far as 2000 m deep (Fig. 10b). Above the bottom layer, the
419 dispersal of the suspended particles present in intermediate and deep waters were advected toward
420 the southwest by the general along slope circulation.

421
422 *Resuspension and off-shelf sediment export induced by both waves/currents and trawls* - A simulation
423 with both natural (waves and currents) and anthropogenic (trawling) processes was intended to check
424 if our assumption about the independence on sediment transport was justifiable. By comparison with
425 the sum of both processes, the annual resuspension and deposition on the shelf due to the combined
426 effect of waves/currents and trawls decrease by ~0.17%, and the off-shelf export did not change
427 (Table 2).

428 The resulting impact of both resuspension processes in the annual change in sediment level is
429 depicted figure 12. By comparison with the impact of each individual resuspension process (Fig. 6 and
430 9), the net erosion/deposition intensity is smoothed all over the shelf. The major areas of net erosion

431 appeared along the coast, on the western outer shelf and around Cape de Creus at the southwestern
432 end of the Gulf. Net sediment accumulation took place over most in the middle shelf and eastern shelf,
433 especially between 20 and 50 m deep.

434 The interaction between the two resuspension processes likely relates to the sediment redistribution
435 on the shelf and to the (simple and irreversible) aggregation mechanism used in the model. Trawling-
436 induced resuspension produces over time a progressive coarsening of the fishing grounds sediments,
437 and a subsequent decrease of the resuspension and deposition fluxes. However, decrease of the
438 deposition flux is slightly lower than that of resuspension because the larger fraction of suspended
439 flocs, build-up from fine (clay and fine silts) sediments, has a higher settling velocity than individual
440 particles and enhances the deposition flux. The impact of bottom trawling activity on the sediment
441 grain size has been already observed. Brown *et al.* (2005) showed on the southeastern Bering Sea
442 that an area protected from bottom trawling, but submitted as the entire coastal region area to natural
443 resuspension, had a significantly finer grain size owing to the lack of winnowing impact of trawling-
444 induced resuspension. Thus some synergist effects between natural and trawling resuspensions exist,
445 but they do only change weakly the net erosion and export fluxes for the Gulf of Lion.

446

447 5. DISCUSSION

448 **Comparison of sediment resuspension by waves/currents and trawls**

449 On average, the amount of sediment resuspended by waves and currents exceeds by 3 to 4 orders of
450 magnitude those induced by trawling (Table 2). By calculating the suspended mass per bottom eroded
451 area for annual and winter/summer periods, a comparison can be made between depths eroded by
452 waves and currents, and by trawls (Fig. 11).

453 Wave and current resuspension flux strongly decreases with increasing water depth, because of the
454 decreasing impact of wave motions, and stabilizes on the outer shelf where strong bottom currents still
455 resuspend muddy sediments (Fig. 11a). Seasonal (winter and summer) fluxes in shallow water are
456 comparable, but summer fluxes decrease more rapidly offshore due to the weaker bottom currents
457 intensity.

458 Resuspension fluxes induced by trawling are maximum on the outer shelf (between 80 and 130 m of
459 depth) and culminate around 100 m depth (Fig. 11b). Seasonally, fluxes are weaker during the winter
460 period by a factor of about 2, because bad sea conditions reduce the average number of sea trips
461 (Fig. 3d). On a yearly basis, resuspension fluxes generated by trawls on the outer shelf are lower than
462 the fluxes generated at the same depths by waves and currents. However, the trawling-induced fluxes
463 significantly exceed the waves and current-induced fluxes during summertime.

Formatted: Bullets and Numbering

464 Churchill *et al.* (1989) suggested, using a simple model, that wave and current on the mid-Atlantic
465 Bight were responsible for the resuspension on the inner shelf shallow water, whereas trawling was
466 the principal cause of resuspension on the outer shelf. Our study shows comparable results and
467 emphasizes the significant impact of bottom trawling on sediment remobilisation in deep regions of
468 continental shelves. However, notable differences appear concerning the intensity of the resuspension
469 fluxes. Indeed, the range of resuspension fluxes by the waves and current (0 - 0.02 kg m⁻²) or trawling
470 (0 - 0.01 kg m⁻²) in the Churchill *et al.* study (1989) is 1 to 3 orders of magnitude weaker than those
471 estimated at similar depths for the Gulf of Lion. Though these fluxes were calculated for different
472 periods (3 months in Churchill *et al.* study (1989), 12 months in our study), the large discrepancy very
473 likely results from different seafloor characteristics, as the Gulf of Lion shelf is mainly made up of fine
474 sediments (clays and silts), whereas sands primarily dominate the seafloor of the Mid-Atlantic Bight.

475

Formatted: Bullets and Numbering

476 **Impact on sedimentary budget**

477 The main export pathways differ for naturally or trawling-induced resuspended sediments because of
478 the different resuspension regions. Waves and currents resuspend sediment mostly on the inner shelf,
479 where it is composed of coarser grains that quickly settle. The fine fraction is then primarily
480 transported along shore toward the southwestern end of the Gulf where it escapes the shelf.
481 Conversely, fine sediment resuspended by trawls is mostly exported to the central slope, owing to the
482 fact that trawled regions are mainly located on the outer shelf, close to the shelf break.

483 Whereas resuspension induced by waves and currents usually dwarfs that induced by trawling, the
484 net erosion (i.e., resuspension-deposition) and the export are more comparable (Table 2). Indeed,
485 sediments resuspended by trawls contribute to about 5% of the annual total export of riverborne and
486 resuspended sediment Gulf of Lion shelf (Table 2 and Fig. 13). Nevertheless, this export shows an
487 important seasonal and interannual variability due to the storm frequency and intensity, resulting in a
488 variable contribution of trawling to the export.

489 During summertime the effect of waves and currents is minimal while the activity of trawling is
490 maximum. Quantitatively, these conditions induce an increased contribution of the trawling impact,
491 which reaches 7% of the total export for the period April 98-September 98. During wintertime the
492 contribution of trawling is minimum around 4%.

493 Ulises *et al.* (submitted) estimated – using a similar modelling approach - a sediment resuspension and
494 export by waves and currents for the Gulf of Lion for the November 2003 - May 2004 period. This
495 latter period was characterized by large river discharges and E-SE storm activity, with the occurrence
496 of one major flood and two extreme storms, but mild dense water formation and export. It was quite
497 different from the low river discharges, low E-SE storm activity, but massive dense shelf water
498 cascading 1998-1999 winter period addressed in the present study. The amount of sediment exported
499 during comparable time period reveals that the export during the November 2003 and March 2004
500 period (8.6×10^6 T) was larger than during the 1998-1999 period (5.7×10^6 T between November 1998 –
501 March 1999). These two periods were very energetic and are believed to represent the upper range of

502 the export. On the other side, Durrieu de Madron *et al.* (2000) estimated from a box model budgeting
503 approach based on direct measurements performed during two seasonal surveys, an annual export of
504 suspended particulate matter of about 1.9×10^6 T. This crude estimate is believed to represent the
505 lower range of the export, as surveys were performed in 1995-1996 during relatively calm conditions.
506 Assuming that the export of sediment associated to the trawling activity is relatively constant from one
507 year to the other (i.e., of the order of 0.4×10^6 T), we estimated that this activity could contribute
508 between few and 20 percents of the annual exchange of suspended sediment at the scale of the Gulf.

509

510 **SUMMARY**

511 Resuspension and transport of sediment in the Gulf of Lion, due to waves and currents on one hand,
512 and to trawling on the other hand, have been modelled for an annual period (April 1998 – April 1999).
513 The major conclusions that can be drawn with these results are:

514 - Natural resuspension by waves and currents occurred during short episodes mostly during fall and
515 winter. It was concentrated on the inner-shelf due to wave action, but also on the southwestern
516 outer shelf due to the strong bottom currents occurring during wintertime. Trawling-induced
517 resuspension occurred regularly throughout the year. It was concentrated on the outer shelf, with a
518 maximum intensity around 90 m depth. Trawling-induced resuspension fluxes are on average
519 several orders of magnitude lower than the waves and currents-induced resuspension fluxes.
520 Nevertheless, they are maximum and locally predominant during summertime when the wave and
521 currents activity is lowest.

522 - The total annual off-shelf export of sediment by waves and currents were one order of magnitude
523 larger than the export linked to trawling. Export concerned the finest fraction of the sediment (clays
524 and fine silts) and took place primarily in the southwestern end of the Gulf for the sediment
525 resuspended by waves and currents and the central shelf for the sediment resuspended by
526 trawling. During energetic years (i.e., with large flood, strong marine storm or dense water
527 formation), the trawling activity contributed little (few percents) to the total shelf export of fine
528 sediment. However, trawling was thought to contribute significantly (up to 20% of the export)
529 during calm years.

530 - No significant interferences between both resuspension processes were estimated in term of
531 resuspension/deposition and export fluxes.

532

533 **ACKNOWLEDGMENTS**

534 The authors acknowledge the support from the European Commission (INTERPOL project under
535 contract EVK3-2000-00023 and EUROSTRATAFORM project under contract EVK3-CT-2002-00079).

537 **REFERENCES**

- 538 Agrawal, Y.C., Pottsmith, H.C. 2000. Instruments for particle size and settling velocity observations in
539 sediment transport. *Marine Geology*, 168, 89-114
- 540 Amos, C.L., Daborn, G.R., Christian H.A. 1992 In situ erosion measurements on fine-grained
541 sediments from the Bay of Fundy. *Marine Geology*, 108, 175-196.
- 542 Amos, C.L., Feeney, T., Sutherland, T.F., Luternauer, J.L. 1997. The stability of fine grained
543 sediments from the Fraser River delta. *Estuarine, Coastal and Shelf Science*, 45, 507-524.
- 544 Arakawa, A. & Suarez, M.J. 1983. Vertical differencing of the primitive equations in sigma coordinates,
545 *Monthly Weather Review*, 111, 34-45.
- 546 Auclair, F., Marsaleix, P., Estournel C., 2000. Sigma coordinate pressure gradient errors : Evaluation
547 and reduction by an inverse method. *Journal of Atmospheric and Oceanic Technologies*, 17, 1347-
548 1367.
- 549 Béthoux, J.P., Durrieu de Madron, X., Nyffeler, F., Tailliez, D. 2002. Deep water in the western
550 Mediterranean : peculiar 1999 and 2000 characteristics, shelf formation hypothesis, variability since
551 1970 and geochemical inferences. *Journal of Marine Systems*, 33-34, 117-131.
- 552 Black, K.S. 1997. Microbiological factors contributing to erosion resistance in natural cohesive
553 sediments. In: Burst, N., Parker, R. and Watts, J., Editors. *Cohesive sediments*, John Wiley & Sons
554 Ltd, Chichester, pp. 231-244.
- 555 Blumberg, A.F., Mellor, G., 1987. A description of a three dimensional coastal circulation model, In :
556 *Three Dimensional Coastal Ocean Model*, edited by N. Heaps, 208 pp.
- 557 Bougeault, P., Lacarrere, P. 1989. Parameterisation of orography-induced turbulence in a meso-beta
558 scale model, *Monthly Weather Review*, 117, pp. 1872-1890.
- 559 Bourrin, F., Durrieu de Madron, X., Ludwig, W., 2007. Contribution to the study of coastal rivers and
560 associated prodeltas to sediment supply in Gulf of Lions (N-W Mediterranean Sea). *Vie et Milieu. Life*
561 *and Environment*. In press.
- 562 Brown E.J., Finney, B., Dommissé, M., Hills, S. 2005. Effects of commercial otter trawling on the
563 physical environment of the southeastern Bering Sea. *Continental Shelf Research*, 25, 1281-1301.
- 564 Canals, M., Puig, P., Durrieu de Madron, X., Heussner, S., Palanques, A., Fabrè J. 2006. Flushing
565 submarine canyons. *Nature*, 444, 354-357.
- 566 Churchill, J.H. 1989. The effect of commercial trawling on sediment resuspension and transport over
567 the Middle Atlantic Bight continental shelf. *Continental Shelf Research*, 9, 841-864.
- 568 DeAlteris, J., L. Skrobe and C. Lipsky. 1999. The significance of seabed disturbance by mobile fishing
569 gear relative to natural processes: a case study in Narragansett Bay, Rhode Island. In L.R. Benaka,
570 editor. *Fish Habitat: Essential fish habitat and rehabilitation*. American Fisheries Society, Symposium
571 22, Bethesda, Maryland, 224-237
- 572 Dufau-Julliard, C., Marsaleix, P., Petrenko, A., Dekeyser, I. 2004. 3D modeling of the Gulf of Lion's
573 hydrodynamics (NW Med.) during January 1999 (MOOGLI3 experiment) and late winter 1999 : WIW
574 formation and cascading over the shelf break. *Journal of Geophysical Research*.109, C11002,
575 doi:10.1029/2003JC002019.
- 576 Durrieu de Madron, X., Nyffeler, F., Godet, C.H. 1990. Hydrographic structure and nepheloid spatial
577 distribution in the Gulf of Lions continental margin. *Continental Shelf Research*, 10, 915-929.
- 578 Durrieu de Madron, X., Abassi, A., Heussner, S., Monaco, A., Aloisi, J.C., Radakovitch, O., Giresse,
579 P., Buscaïl, R., Kerhervé, P. 2000. Particulate matter and organic carbon budgets for the Gulf of Lions
580 (NW Mediterranean). *Oceanologica Acta*, 23 (6), 717-730
- 581 Durrieu de Madron, X., Denis, L., Diaz, F., Garcia, N., Guieu, C., Grenz, C., Loÿe-Pilot, M.D., Ludwig,
582 W., Moutin, T., Raimbault, P., Ridame, C. 2003. Nutrients and carbon budgets for the Gulf of Lion
583 during the Moogli cruises. *Oceanologica Acta*, 26, 421-433.

- 584 Durrieu de Madron X., Ferré, B., Le Corre, G., Grenz, C., Conan, P., Pujo-Pay, M., Bodirot, O., Buscail,
585 R. (2005) Trawling-induced resuspension and dispersal of muddy sediments and dissolved elements.
586 *Continental Shelf Research*, 25 (19-20), 2387-2409.
- 587 Dyer, K.R. 1986. *Coastal and Estuarine Sediment Dynamics*, John Wiley and Sons, London.
- 588 El Ganaoui O., Schaaff E., Boyer P., Amielh M., Anselmet F. and Grenz C. (2004) The deposition and
589 erosion of cohesive sediments determined by a multi-class model. *Estuarine, Coastal and Shelf*
590 *Science*, 60 (3), 457-475
- 591 Estournel, C., Kondrachoff, V., Marsaleix, P., Vehil, R. 1997. The plume of the Rhône : numerical
592 simulation and remote sensing, *Continental Shelf Research*, 17, 899-924.
- 593 Estournel, C., Broche, P., Marsaleix, P., Devenon, J.L., Auclair, F., Vehil, R. 2001. The Rhone river
594 plume in unsteady conditions : numerical and experimental results. *Estuarine, Coastal and Shelf*
595 *Science*, 53, 25-38.
- 596 Estournel, C., Durrieu de Madron, X., Marsaleix, P., Auclair, F., Julliand, C., Vehil, R. 2003.
597 Observations and modelisation of the winter coastal oceanic circulation in the Gulf of Lions under wind
598 conditions influenced by the continental orography (FETCH experiment). *Journal of Geophysical*
599 *Research*, 108(C3), p. 8059.
- 600 Ferré, B., Guizien, K., Durrieu de Madron, X., Palanques, A., Guillén, J., Grémare, A. 2005. Fine
601 sediment dynamics study during a winter storm in the Gulf of Lion shelf (NW Mediterranean), en
602 révision à *Continental Shelf Research*. *Continental Shelf Research*, 25 (19-20), 2410-2427.
- 603 Garcia-Estevez, J. 2005. Transferts géochimiques en Méditerranée : exemple de la rivière Têt et de
604 son bassin versant. Ph.D. Thesis, University of Perpignan, pp 263.
- 605 Geernaert, G.L. 1990. Bulk parameterizations for the wind stress and heat fluxes. In: Geernaert and
606 Plant (Eds.), *Surface waves and fluxes. Volume I -Current theory*. Kluwer Academic Publishers, pp.
607 336.
- 608 Grant, W.D., Madsen, O.S., 1982. Movable bed roughness in unsteady oscillatory flow. *Journal of*
609 *Geophysical research*, 87, 469-481.
- 610 Guillén J., Bourrin, F., Palanques, A., Durrieu de Madron, X., Puig, P., Buscail, R. 2006. Sediment
611 dynamics during "wet" and "dry" storm events on the Têt inner shelf (SW Gulf of Lions). *Marine*
612 *Geology*, 234, 129-142.
- 613 Gust, G., Morris, M.J. 1989. Erosion thresholds and entrainment rates of undisturbed in situ
614 sediments. *Journal Coastal Research*, 5, 87-99.
- 615 Harris, C.K, Wiberg, P.L. 2001. A two-dimensional, time-dependent model of suspended sediment
616 transport and bed reworking for continental shelves. *Computers and Geosciences*, (27), 675-690.
- 617 Heussner S., Durrieu de Madron, X., Calafat, A., Canals, M., Carbonne, J., Delsaut, N., Saragoni, G.,
618 2006. Spatial and temporal variability of downward particle fluxes on a continental slope: lessons from
619 an 8-yr experiment in the Gulf of Lions (NW Mediterranean). *Marine Geology*, 234, 63-92
- 620 Hill, P.S., Syvitski, J.P., Cowan, E.A., Powell, R.D., 1998. In situ observations of floc settling velocities
621 in Glacier Bay, Alaska. *Marine Geology*, 145, 85-94.
- 622 Houwing, E.J. 1999. Determination of the critical erosion threshold of cohesive sediments on intertidal
623 mudflats along the Dutch Wadden sea coast. *Estuarine, Coastal and Shelf Science*, 49, 545-555.
- 624 Houwing, E.J. 2000. Sediment dynamics in the pioneer zone in the land reclamation area of the
625 Wadden Sea, Groningen, The Netherlands. Ph.D. Thesis, University of Utrecht, Utrecht.
- 626 Krishnappan, B.G., Marsalek, J., 2002. Transport characteristics of fine sediment from an on-stream
627 stormwater management pond. *Urban Water*, 4, pp. 3-11.
- 628 Lapouyade, A., Durrieu de Madron, X., 2001. Seasonal variability of the advective transport of
629 particulate matter and organic carbon in the Gulf of Lion (NW Mediterranean). *Oceanologica Acta*, 24,
630 295-312.
- 631 Li, M.Z., Amos, C.L. 1998. Predicting ripple geometry and bed roughness under combined waves and
632 currents in a continental shelf environment. *Continental Shelf Research*, 18(9), 941-970.

- 633 Li, M.Z., Amos, C.L. 2001. SEDTRANS96 : the upgraded and better calibrated sediment-transport
634 model for continental shelves. *Computers and Geosciences*, (27), 619-645.
- 635 Maa, J.P., Sanford, L., Halka, J.P. 1998. Sediment resuspension characteristics in Baltimore Harbor,
636 Maryland. *Marine Geology*, 146, 137-145
- 637 Marsaleix, P., Estournel, C., Kondrachoff, V., Vehil, R. 1998. A numerical study of the formation of the
638 Rhone river plume. *Journal of Marine Systems*, 14, 99-115.
- 639 Meadows, P.S., Tait, J., Hussain, S.A. 1990. Effects of estuarine infauna on sediment stability and
640 particle sedimentation. *Hydrobiologia*, 190, 263-266.
- 641 Millot, C., 1999. Circulation in the western Mediterranean Sea. *Journal of Marine Systems*, 20 (1-4),
642 423-442.
- 643 Monaco, A., Durrieu de Madron, X., Radakovitch, O., Heussner, S. & Carbonne, J. 1999. Origin and
644 variability of downward biogeochemical fluxes on the Rhône continental margin (NW Mediterranean). -
645 *Deep-Sea Research I*, 46, 1483-1511.
- 646 Mulder, H.P., Udink, C. 1991. Modelling of cohesive sediment transport. A case study: the western
647 Scheldt estuary. In: Edge, B.L. Editor. *Proceedings of the 22nd International Conference on Coastal
648 Engineering*, ASCE, 3012-3023.
- 649 Nielsen, P. 1986. Suspended sediment concentrations under waves. *Coastal Engineering*, 10, 23-31?
- 650 Oey, L.Y., Chen, P. 1992. A model simulation of circulation in the northeast Atlantic shelves and seas.
651 *J. Geophys. Res.*, 97, 20,087-20,115
- 652 Palanques, A., Durrieu de Madron, X., Puig, P., Fabres, J., Guillén, J., Calafat A., Canals, M.,
653 Heussner, S., Bonnin, J. 2006. Suspended sediment fluxes and transport processes in the Gulf of
654 Lions submarine canyons. The role of storms and dense water cascading. *Marine Geology*, 234, 43-
655 61.
- 656 Palanques, A., Puig, P., Guillén, J., Jiménez, J., Gracia, V., Sánchez-Arcilla, A. and Madsen, O.
657 2002. Near-bottom suspended sediment fluxes on the microtidal low-energy Ebro continental shelf
658 (NW Mediterranean) *Continental Shelf Research*, 22, 285-303.
- 659 Panagiotopoulos, I., Voulgaris, G., Collins, M.B. 1997, The influence of clay on the threshold of
660 movement on fine sandy beds, *Coastal Engineering*, 32, 19-43.
- 661 Partheniades, E. 1962. A study of erosion and deposition of cohesive soils in salt water. Ph. D. Thesis.
662 University of California, Berkeley, 182 pp.
- 663 Pethélet-Giraud, E., Negrel, P.-H., Cubizolles, J., 2003. Flux exportés de l'Hérault vers la
664 Méditerranée et origine des masses d'eau. Rapport BRGM /RP-52748-FR.
- 665 Petrenko, A., Leredde, Y., Marsaleix, P., 2004. Circulation in a stratified and wind-forced Gulf of Lions,
666 NW Mediterranean Sea: in situ and modelling data. *Continental Shelf Research*, 25 (1), 7-27.
- 667 Poirel, A., Carrel, G., Olivier, J.M., 2001. Illustration de la complémentarité des chroniques
668 environnementales dans l'étude d'un hydrosystème fluvial : régime thermique et peuplements
669 piscicoles du Rhône, Workshop "Activities in the catchment area and water quality", Lyon Fleuves
670 2001, juin 2001.
- 671 Schaaff, E., Grenz, C., Pinazo, C., 2002. Erosion of particulate inorganic and organic matter in the
672 Gulf of Lion. *Comptes Rendus Géosciences*, 334, 1071-1077.
- 673 Sempéré R., Charrière B., Van Wambeke F. and Cauwet G. (2000) Carbon inputs of the Rhone River
674 to the Mediterranean Sea: Biogeochemical implications. *Global Biogeochemical Cycles*, 14, 669-681.
- 675 Serrat, P. 1999. Present sediment yield from a Mediterranean fluvial system: the Agly river (France).
676 *Comptes Rendus de l'Académie des Sciences - Series IIA - Earth and Planetary Science*. 329,189-
677 196.
- 678 Serrat, P., Ludwig, W., Navarro, B., Blazi J.L., 2001. Spatial and temporal variability of sediment fluxes
679 from a coastal Mediterranean river: the Têt (France). *Comptes Rendus de l'Académie des Sciences -
680 Series IIA - Earth and Planetary Science*, 333, 389-397.

- 681 Soulsby, R.L., Hamm, L., Klopman, G., Myrhaug, D., Simons, R.R., Thomas G.P. 1993. Wave-current
682 interaction within and outside the bottom boundary layer. *Coastal Engineering*, 21, 41-69.
- 683 Soulsby, R.L., Whithouse, R.J.S.W. 1997. Threshold of sediment motion in coastal environments.
684 *Proceedings Pacific Coasts and Ports '97 Conference*, Christchurch, 1, 149-154.
- 685 Torfs, H. 1995. Erosion of mud/sand mixtures. Ph.D. thesis, Katholieke Universiteit Leuven, faculteit
686 der Toegepaste Wetenschappen, Departement Burgelijke Bouwkunde, Laboratorium voor Hydraulica.
- 687 Ulses, C., Estournel, C., Bonnin, J., Durrieu de Madron, X., Marsaleix, P. Impact of storms and dense
688 water cascading on shelf-slope exchanges in the Gulf of Lion (NW Mediterranean). *Journal of*
689 *Geophysical Research* (accepted).
- 690 Ulses, C., Estournel, C., Durrieu de Madron, X., Palanques, A. Suspended sediment transport in the
691 Gulf of Lion (NW Mediterranean) : Impact of extreme flood and storm. *Continental Shelf Research*
692 (submitted)
- 693 Wentworth, C.K. 1922. A scale of grade and class terms for clastic sediments, *Journal of Geology*, 30,
694 377-392.
- 695 Wheatcroft, R.A. 1994. Temporal variation on bed configuration and one-dimensional bottom
696 roughness at the mid-shelf STRESS site. *Continental Shelf research*, 14, 1167-1190.
- 697 Widdows, J., Brinsler, M.D., Bowley, N., Barrett C., 1998. A benthic annular flume for in situ
698 measurement of suspension feeding/biodeposition rates and erosion potential of intertidal cohesive
699 sediments. *Estuarine, Coastal and Shelf Sciences*, 46, 27-38.1998
- 700 Zanke, U. 1977. Berechnung der Sinkgeschwindigkeiten von Sedimenten. *Mitteilungen des Franzius-*
701 *Institutes*, 46, 231-245.
- 702 Zyserman, J.A., Fredsøe, J., 1994. Data analysis of bed concentration of suspended sediment.
703 *Journal of Hydraulic Engineering*, ASCE, 120 (9), 1021-1041.

704 **APPENDIX 1**

705 *Suspended sediment transport equation*

706 The advection-diffusion equation is based on the mass conservation of the suspended sediment

$$\frac{\partial C^i}{\partial t} + u \frac{\partial C^i}{\partial x} + v \frac{\partial C^i}{\partial y} + (w - W_s^i) \frac{\partial C^i}{\partial z} = K_z \frac{\partial^2 C^i}{\partial z^2} \quad (1)$$

707 where C^i is the suspended sediment concentration (SSC) for the i^{th} class of particles, W_s^i is the settling
708 velocity, u , v and w are the horizontal and vertical velocity respectively and K_z is the vertical diffusion
709 coefficient.

710

711 The vertical turbulence was estimated using a turbulent closure scheme where the vertical diffusion

712 coefficient K_z is derived from the local Richardson number $\left(Ri = -\frac{(g/\rho)(\partial\rho/\partial z)}{(\partial u/\partial z)^2} \right)$:

$$K_z = 1.67 \times 10^{-3} \left(1 + \frac{10}{3} Ri \right)^{-3/2} \quad (2)$$

713 where ρ is the water density and g is the gravitational acceleration equal to $9.81 \text{ m}^2 \text{ s}^{-1}$.

714

715 Settling velocity W_s^i (in m s^{-1}) for the particles with a diameter lower than $100 \text{ }\mu\text{m}$ was estimated as the
716 mean Stokes velocity of the individual size bins D_j (in m):

$$W_s^i = \frac{(s_i - 1)gD_i^2}{18\nu} \quad (3)$$

717 where s_j is the relative grain density and ν is the kinematic water viscosity equal to $1.14 \times 10^{-6} \text{ m}^2 \text{ s}^{-1}$.

718 Settling velocity for sand grain coarser than $100 \text{ }\mu\text{m}$ is computed using Zanke (1977) formula:

$$W_s^i = \frac{10\nu}{D_i} \left\{ \left[1 + \frac{0.01(s_i - 1)gD_i^3}{\nu^2} \right]^{0.5} - 1 \right\} \quad (4)$$

719

720 Settling velocity of aggregates is computed using the relationship from Agrawal and Pottsmith (2000):

$$W_s^i = 0.45 \times 10^{-3} (D_i / 2)^{1.17} \quad (5)$$

721 where W_s^i and D_i are expressed in cm s^{-1} and μm respectively.

722

723 Density of primary particles is taken as the mineral grain density (2640 kg m^{-3}) and density of
724 aggregates is calculated according to Hill *et al.* (1998):

$$\rho_f^i = \rho + \frac{18\mu W_s}{g D_f^2} \left(1 + \frac{3C}{16} \text{Re} \right) \quad (6)$$

725 where ρ_f^i is the aggregate density, μ is the dynamic water viscosity ($1.14 \times 10^{-3} \text{ kg m}^{-1} \text{ s}^{-2}$), W_s is the
726 aggregate settling velocity, D_f is the aggregate diameter, C is the Carrier coefficient (0.43) and
727 $\text{Re} = \rho W_s^i D_f^i / \mu$ is the class i Reynolds number.

728 **APPENDIX 2**

729 *Erosion fluxes*

730 *Partheniades' law for cohesive sediments* - It permits to calculate the erosion flux F for each particle
731 class i according to the relation:

$$F^i = p_i E_0^i \left(\frac{\tau_{\max,s}}{\tau_{cf_i}} - 1 \right) \text{ if } \tau_{\max,s} \geq \tau_{cf_i} \quad (7)$$

732 where τ_{cf_i} is the critical shear stress for the class i and p_i is the fraction of class i . The erosion
733 coefficient E_0 depends on the physico-chemical sediment characteristics and ranged between 10^{-5}
734 and $2 \cdot 10^{-3} \text{ kg m}^2 \text{ s}^{-1}$ (Mulder et Udink, 1991; Amos *et al.*, 1992; Amos *et al.*, 1997, Widdows *et al.*,
735 1998). In this study, the coefficient E_0 was set to $1 \cdot 10^{-5} \text{ kg m}^2 \text{ s}^{-1}$

736

737 *Reference concentration method for non-cohesive sediments* – It permits to calculate the erosion flux
738 F for each particle class i according to the relation:

$$F^i = p_i W_s^i C(z_i) \rho_s^i \quad (8)$$

739 where $C(z_i)$ is an adimensional concentration at the height z_i corresponding to the first layer of the
740 grid of above the seabed. Under combined wave and currents conditions, sediment is resuspended
741 within the wave boundary layer and diffused in the water column by turbulence associated with the
742 current (Soulsby *et al.*, 1993). In the model, height of the first layer (z_i) is variable and can be above
743 the wave boundary layer of thickness z_w . The concentration $C(z_i)$ is thus calculated according to the
744 reference concentration C_a , at height $z_a = 2D_{50}$, or the concentration at the boundary layer level $C(z_w)$.

$$C(z_1) = C_a \left(\frac{z_1}{z_a} \right)^{-b_{\max}} \quad \text{for } z_a \leq z_1 \leq z_w \quad \text{with } b_{\max} = \frac{W_s}{\kappa u_{\max}} \text{ and } b_m = \frac{W_s}{\kappa u_m}$$

$$C(z_1) = C(z_w) \left(\frac{z_1}{z_w} \right)^{-b_m} \quad \text{for } z_w < z_1 \quad z_w = \frac{W_s T}{2\pi} = \text{wave boundary thickness}$$

745 W_s is the sediment settling velocity, κ is the von Karman constant ($= 0.40$), $u_{\max} = (\tau_{\max} / \rho)^{1/2}$, $u_m = (\tau_m$
746 $/ \rho)^{1/2}$, τ_{\max} is the maximum bed shear-stress in wave cycle, τ_m is the mean bed shear-stress in wave
747 cycle, and T the wave period.

748 The determination of the reference concentration is based on Zyserman and Fredsøe (1994) method,
 749 and is calculated for a grain-related roughness height of $2.5 \times D_{50}/30$:

$$C_a = \frac{0.331 (\theta_{\max,s} - 0.045)^{1.75}}{1 + 0.720 (\theta_{\max,s} - 0.045)^{1.75}} \quad (9)$$

750 Where $\theta_{\max,s} = \frac{\tau_{\max,s}}{g(\rho_s - \rho)D_{50}}$ is the skin-friction Shields parameter.

751 The latter method is designed for flat-bed condition, so that τ_{\max} and τ_m are calculated using a grain
 752 related roughness height ($2.5 \times D_{50}/30$). For a rippled bed, total-stress values should be used.

753 *Erosion flux for trawl* – The fluxes of sediment resuspended by bottom trawls were estimated by
 754 Durrieu de Madron *et al.* (2005). They showed that resuspension by trawl depend on the trawl's
 755 goundrope gear, but above all on the sediment texture (clay content). They inferred a linear
 756 relationship between the total resuspension flux, E_T in $\text{kg m}^{-2} \text{s}^{-1}$, and the clay fraction, F_c in %:

$$E_T = 0.011 F_c + 0.47 \quad (r^2 = 0.74)$$

757 Total flux is then fractionated for the different sediment grain sizes, according to the fraction p_i of class
 758 i .

$$F^i = p_i E_T$$

759
 760

761 *Critical shear stress*

762 The critical shear stress is the shear stress from which sediment is likely to be removed. It depends on
 763 the grain itself and on bottom characteristics. This value is difficult to establish because it can vary
 764 from a factor 10 to 20 according to the type of resuspension considered.

765 For coarse non-cohesive sediments which mainly depend on grain characteristics, critical shear stress
 766 of each class i is given in form of a critical Shields parameter value θ_{cr}^i which depends on
 767 adimensional grain size and results from experiments. Soulsby and Whithouse (1997) determined an
 768 algebraic equation nearest to the Shields curve:

$$\theta_{cr}^i = \frac{0.30}{1 + 1.2D_*^i} + 0.055 \left[1 - e^{-0.020D_*^i} \right] \text{ where } D_*^i = \left[\frac{g(s^i - 1)}{\nu^2} \right]^{1/3} D_{50}^i \quad (10)$$

769 Critical shear stress τ_{cr}^i is thus calculated with the equation

$$\theta'_{cr} = \frac{\tau'_{cr}}{g(\rho'_s - \rho)D'_{50}} \quad (11)$$

770

771 *Roughness and bedforms*

772 For non-cohesive sediments, total bottom roughness is computed using the relationship

$$z_b = k/30 \quad (12)$$

773 where k is the total roughness height, and is the sum of three components: grain-related component
 774 (k_g), bedload component (k_l), and form-drag component (k_f) (Grant and Madsen, 1982).

$$k = k_g + k_l + k_f \quad (13)$$

775 Grain roughness height is calculated using:

$$k_g = 2.5 \times D_{50} \quad (14)$$

776 Bedload roughness is calculated using:

$$k_l = 522 \times D_{50} (\theta_{cws} - \theta_{cr})^{0.75} \quad (15)$$

777 where $\theta_{cws} = \rho u_{cws}^2 / (\rho_s - \rho) g D_{50}$ is the Shields parameter related to the skin roughness, θ_{cr} is the
 778 critical Shields parameter which define grains remobilization, and U_{cws} is combined wave and currents
 779 shear velocities.

780 The ripple height and wavelength is then calculated according to Li and Amos (1998) (see below) to
 781 obtain the form drag roughness height

782

$$k_f = a_r \eta^2 / \lambda \quad (16)$$

783 where a_r is a coefficient which varies according to authors. We choose 27.7, the most common value,
 784 fixed by Grant and Madsen (1982).

785 The ripple height and wavelength depend on the characteristic and hydrodynamical conditions. Skin
 786 shear velocities (u_{cws}^*) and skin-friction combined wave and current Shields parameter (θ_{cws}) are first
 787 calculated using the grain roughness height k_g . The bedload roughness k_l can thus be calculated, and
 788 is used to obtain bedload shear velocities (u_{wt}^* , u_{ct}^* , u_{cwt}^*). To calculate ripples dimension, the
 789 combined-flow ripple predictor proposed by Li and Amos (1998), based on their filed observations of
 790 ripples on Scotian Shelf, is used. Ripple dimensions are calculated according to five limit condition for

791 friction velocities: ripple-enhanced shear velocity (u_{cwe} , Nielsen, 1986), critical shear velocity for
 792 bedload transport (u_{cr}), critical shear velocity for ripple break-off (u_{bf} , Grant and Madsen, 1982) and
 793 critical shear velocity for upper-plane bed sheet-flow (u_{up}). This last variable is given from a data
 794 compilation from preceding studies, carried out by Li and Amos (1998).

795 $u_{cwe} = u_{cws} / (1 - \pi \eta_p / \lambda_p)$ where η_p and λ_p are respectively height and wavelength of pre-existing
 796 ripples.

797 $u_{cr} = \sqrt{\tau_{cr} / \rho}$, τ_{cr} being the critical shear stress for erosion as explain hereafter.

798 $u_{bf} = 1.34 S_*^{0.3} u_{cr}$ where $S_* = (D_{50} / 4\nu) [(\rho_s - \rho) g D_{50} / \rho]$ is without dimension and ν is the
 799 cinematic seawater viscosity (equal to 1.14×10^{-6} for a 15°C seawater).

800 $u_{up} = \sqrt{\tau_{up} / \rho}$ where $\tau_{up} = \theta_{up} (\rho_s - \rho) g D_{50}$ and $\theta_{up} = 0.172 D_{50}^{-0.125}$, D_{50} is expressed in mm.

801 The five limit conditions are presented above and permit to determine the adapted equations to
 802 calculate ripples height η_{rip} and wavelength λ_{rip} :

803 - If $u_{cwe} < u_{cr}$, there is no sediment transport and ripples have the same dimension as precedent time
 804 step.

805 - If $u_{cwe} > u_{cr}$ and $u_{cws} < u_{cr}$, the transport is local, weak, and close to ripples crest.

806 • $\eta_{rip} / D_{50} = 19.59 (u_{cws} / u_{cr}) + 20.92$

807 • $\eta_{rip} / \lambda_{rip} = 0.12$

808 - If $u_{cws} > u_{cr}$ and $u_{cwt} < u_{bf}$, overall bedload transport will occur.

809 case n°1 : $u_{cw} / u_{cs} \geq 1.25$, wave-dominant ripples

810 ○ $\eta_{rip} / D_{50} = 27.14 (u_{cwt} / u_{cr}) + 16.36$

811 ○ $\eta_{rip} / \lambda_{rip} = 0.12$

812 case n°2 : $u_{cw} / u_{cs} < 1.25$, current-dominant ripples or interaction between wave and currents

813 ○ $\eta_{rip} / D_{50} = 22.15 (u_{cwt} / u_{cr}) + 6.38$

814 ○ $\eta_{rip} / \lambda_{rip} = 0.12$

815 - If $u_{bf} \leq u_{cwt} < u_{up}$, break-off ripples will form

816 - $\lambda_{rip} = 535 D_{50}$

817 - $\eta_{rip} / \lambda_{rip} = 0.15 (u_{up} - u_{cwt}) / (u_{up} - u_{bf})$

818 - If $u_{cwt} \geq u_{up}$, ripples are washed out and upper-plane bed will be predicted.

819 - $\eta_{rip} = 0$

820 - $\lambda_{rip} = 0$

821 From these ripples height and wavelength values, the drag roughness, and then the total bottom
822 roughness can be calculated, giving access to the calculation of the bottom shear stress which will
823 determine the reference concentration.

824

825 For cohesive sediment, biological activity can have a considerable effect on bottom roughness.
826 Microbial exudates can increase the critical shear stress, and presence of burrows in the sediment,
827 due to bioturbation, can strengthen the seabed (Meadows *et al.*, 1990; Black, 1997). Data concerning
828 biological roughness being non-existent in the Gulf of Lion, ripples height and the wavelength for
829 3.6cohesive sediment are selected here equal to those measured on a silty site in the North-East of
830 California, that says 0.6 cm and 10 cm respectively (Wheatcroft, 1994). The steepness of biogenic
831 roughness elements is assumed to decay under high shear stresses as:

$$\frac{\eta_{bio}}{\lambda_{bio}} = \exp(-1.67 \ln \theta_w - 4.11) \quad (\text{Harris and Wiberg, 2001}) \quad (17)$$

832 where $\theta_w = \tau_{*w} / g(\rho_s - \rho)D_{50}$.

833 For mixed sediment, an average between silty-bed and sandy-bed roughness scale is used, weighted
834 by sand fraction of the bed (Harris et Wiberg, 2001) :

$$\begin{aligned} \eta &= \eta_{rip} f_{r_s} + \eta_{bio} (1 - f_{r_s}) \\ \lambda &= \lambda_{rip} f_{r_s} + \lambda_{bio} (1 - f_{r_s}) \end{aligned} \quad (18)$$

835 where f_{r_s} is the sandy fraction. In the same way, total roughness is calculated by weighted average of
836 the cohesive and non-cohesive contributions. A minimum value of $z_0=0.005$ cm is specified so that
837 roughness estimates do not become too small given the small-scale bed variations generally present
838 on the sea floor.

839

840 *Bed armoring*

841 We used the method of Harris and Wiberg (2001), which considers several layers below an active
842 layer available for erosion. Underlying layers are only available when active layer gets thinner by
843 erosion or when shear stress increases. At the initial time, all layers (under-layers and active layer)
844 have the same particle size distribution. The thickness and particle size distribution of each layer are
845 updated at each time step according to deposit and erosion. Volume of each particles class per unit

846 area of eroded seabed during a time step is limited by the quantity of sediment available in the active
847 layer.

848 The active layer of sandy bottom (δ^{rip}) is calculated according to the migration rate of the bottom (Q_b)
849 and the size of the ripples η_{rip} and λ_{rip} during a half wave-period:

$$\delta^{rip} = \frac{Q_b T}{2C_b \lambda_{rip}} + 6D_{50} \quad (19)$$

where $Q_b = \sum_i \left[f r_i \frac{25.3}{(\rho_s^i - \rho) g} (\tau_{cws} - \tau_{cr}^i)^{1.5} \right]$ and $\tau_{cws} = \rho u_{*cws}^2$

850 where $f r_i$ is the fraction of class i present in the sediment, C_b is the concentration of the sediment (1-
851 porosity), and $6D_{50}$ represents irregularities due to grains in order to prevent the active layer to
852 disappear when no transport occurs.

853 For silty sediments, the active layer depth is supposed to be proportional to the shear stress at the
854 bottom compared to the critical shear stresses $\tau_{cr(50)}$ of the sediment.

$$\delta^{silt} = 0.006 (\tau_{cws} - \tau_{cr(50)}) + 6D_{50} \quad (20)$$

855

856 For mixed sediment (mixture of silt and sand), the mixed layer δ_{mix} is calculated as a weighted mean of
857 active layer depths for sandy and silty sediments.

$$\delta_{mix} = \delta^{rip} f r_s + \delta^{silt} (1 - f r_s) \quad (21)$$

858 where $f r_s$ is the sand fraction of the bed. Volume of sediment available for erosion in a size class i per
859 unit area of the bed is $f r_i C_b \delta_{mix}$. This volume is used to limit the erosion, taking into account initial
860 sediment characteristics (critical shear stress for erosion, grain density and particle size distribution).
861 Hence, when erosion exceeded the available sediment volume for each class i at a given site, bed
862 armoring is applied by reducing the flux of this class.

863 **FIGURES CAPTIONS**

864 Figure 1. (a) Topography of the Gulf of Lion in the model and position of hydrological stations. Dash
865 lines delineate different domains used in the text. The line around shelf break depth (200 m) is the limit
866 between the shelf and the open sea. The shelf is subdivided in two halves for water flux estimates
867 given in Fig. 3g. (b) Median grain size of superficial sediment showing the seaward fining texture of the
868 sediment and coarsening around the shelf edge.

869 Figure 2. Probability density distribution of bottom trawls for a) weak wind ($\leq 10 \text{ m s}^{-1}$) and b) strong
870 winds ($>10 \text{ m s}^{-1}$). Black dots indicate the position of fishing ports sheltering the fleet of bottom
871 trawlers: PV (Port-Vendres), PN (Port-la-Nouvelle), A (Agde), S (Sète), GR (Grau du Roi), PB (Port de
872 Bouc). Isobaths 50, 200, 1000 and 2000 m superimposed as black lines.

873 Figure 3. Time series from April 1998 to April 1999 of (a) water discharges from the Rhône River and
874 other rivers of the Gulf of Lion, (b) solid discharge from all rivers, (c) wind off Sète, (d) daily strength of
875 bottom trawls in the Gulf of Lion, (e) bottom shear stress off Marseille and Banyuls (see Fig. 1 for
876 position), (f) water density anomaly at 200 m depth at the eastern end (Planier Canyon) and
877 southwestern end (Cap Creus Canyon) of the Gulf, and (g) and water flux across the shelf break
878 (slope water import onto the shelf is positive, whereas shelf water export is negative).

879 Figure 4. Map of sediment thickness accumulated after a 16-month simulation (January 4, 1998 –
880 March, 31, 1999) taking solely into account sediment discharges from rivers (no resuspension
881 allowed).

882 Figure 5. Annual (from April 1, 1998 to March 31, 1999) variability of the mass of sediment
883 resuspended daily by waves and currents on the shelf (a) and exported towards the slope (b).

884 Figure 6. Map of sediment thickness accumulated or eroded between April 1, 1998 and March 31,
885 1999 taking into account sediment discharges from all rivers and resuspension by waves and currents.
886 The contours are in mm, positive values (light areas) represent deposition and negative values (dark
887 areas) represent erosion.

888 Figure 7. Cross-margin sections on the western part of the Gulf of Lion (see Fig. 1 for section position)
889 showing the distribution of suspended sediment concentration, resuspended by waves and currents,
890 along with water density anomaly in (a) strongly stratified conditions (27 September 1998), and (b)
891 weakly stratified conditions (24 February 1999). The contour unit is mg L^{-1} . The inserted map indicates
892 the location of the cross-slope transect.

893 Figure 8. Annual (from April 1, 1998 to March 31, 1999) variability of the mass of sediment
894 resuspended daily by bottom trawlers on the shelf (a) and exported towards the slope (b).

895 Figure 9. Map of sediment thickness accumulated or eroded between April 1, 1998 and March 31,
896 1999 taking into account sediment discharges from all rivers and resuspension by bottom trawling.
897 The contours are in mm, positive values (light areas) represent deposition and negative values (dark
898 areas) represent erosion.

899 Figure 10. Cross-margin sections on the western part of the Gulf of Lion (see Fig. 1 for section
900 position) showing the distribution of sediment concentration, resuspended by bottom trawling, along
901 with water density anomaly in (a) strongly stratified conditions (27 September 1998), and (b) weakly
902 stratified conditions (24 February 1999). The contour unit is mg L^{-1} . The inserted map indicates the
903 location of the cross-slope transect.

904 Figure 11. Map of sediment thickness accumulated or eroded between April 1, 1998 and March 31,
905 1999 taking into account sediment discharges from all rivers and both resuspension by waves and
906 currents, and bottom trawling. The contours are in mm, positive values (light areas) represent
907 deposition and negative values (dark areas) represent erosion.

908 Figure 12. Annual and seasonal variation with depth of the resuspension fluxes on the Gulf of Lion's
909 shelf linked (a) to natural (wave and current) activity, and (b) to bottom trawling activity. The first 30 m
910 depths are not represented because of the strong erosion by waves and currents very near the coast
911 which dwarfed the other values.

912 Figure 13. Cumulative export (in 10^6 Tons) for the different scenarios: a) natural (waves and currents),
913 b) trawls and c) mixed (waves, currents, and trawls). The dotted line indicates the sum of export for
914 scenarios (a) and (b).

915

916 **TABLE CAPTIONS**

917 Table 1. Characteristics of particle grain size classes used in the sediment transport model.

918 Table 2. Annual sediment fluxes integrated between April 1, 1998 and March 31, 1999. Scenarios with
919 natural (waves and currents) and/or trawling resuspension include sediment input by rivers. Deposition
920 and export rates for these scenarios exclude the deposited and exported sediment directly deriving
921 from rivers. Once riverine sediment has been deposited on the shelf it is accounted in the
922 resuspension, and subsequent deposition and export fluxes.

Table 1. Characteristics of particle grain size classes used in the sediment transport model

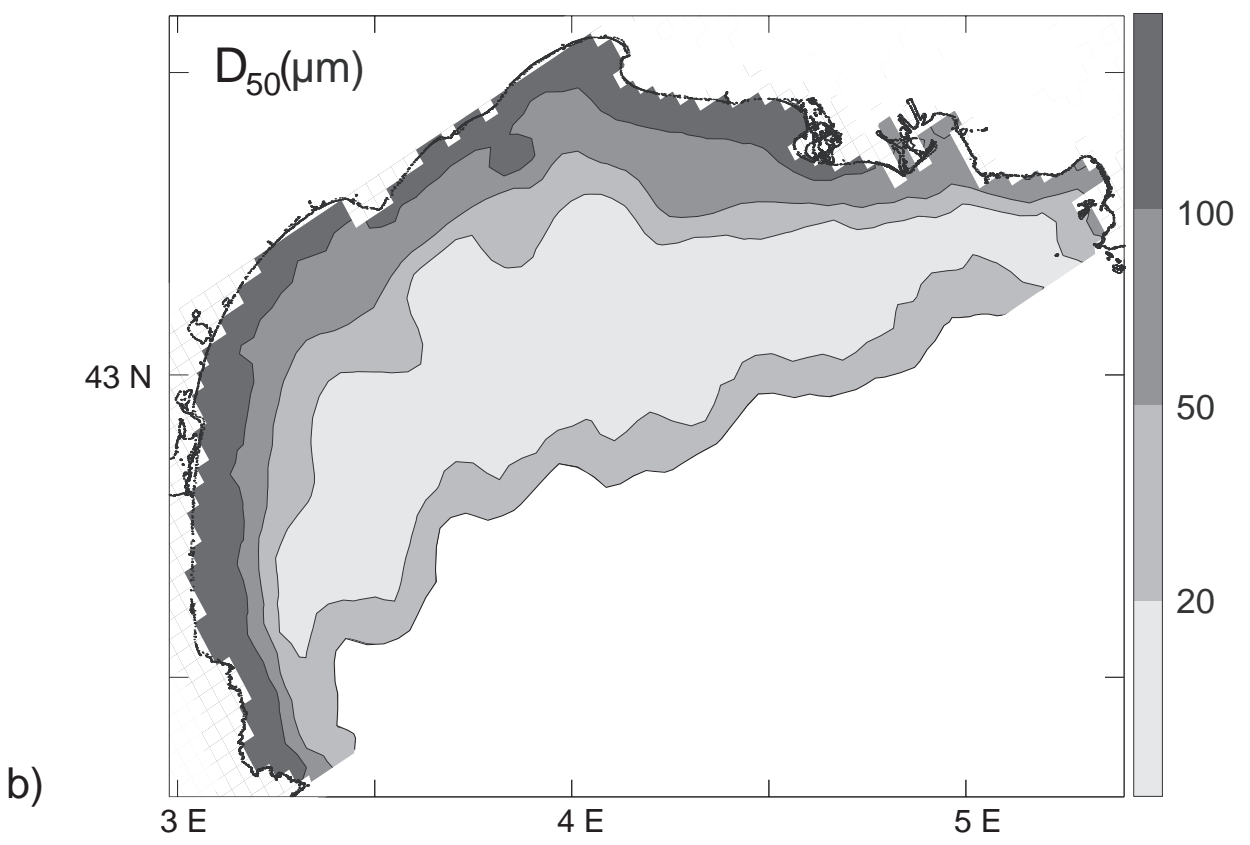
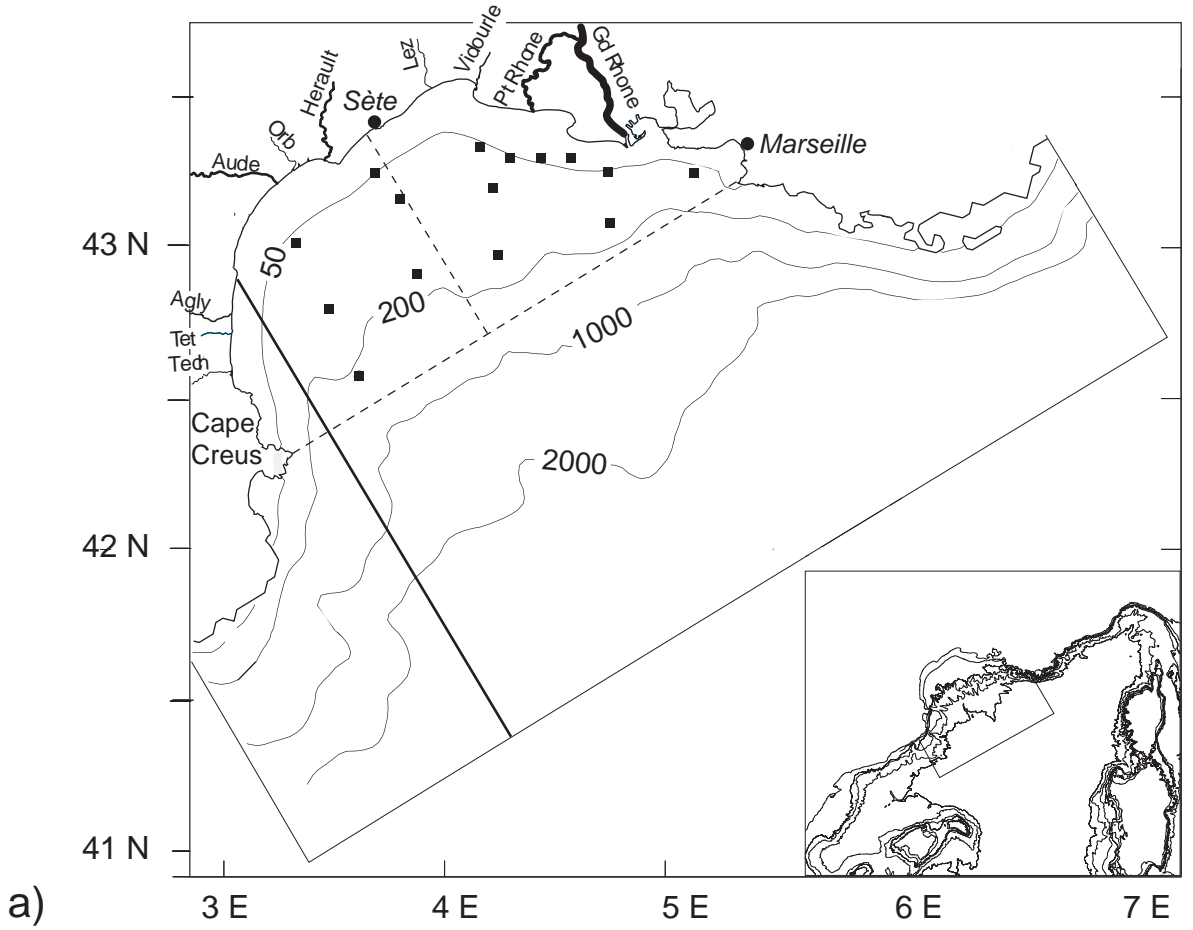
Class	1	2	3	4	5	6	7	8	9
category	clay	Fine silt	Coarse silt	Very fine sand	Fine sand	Median sand	Coarse sand	Aggregates	
D_{50} (μm)	2.43	8.39	31.6	92.4	179.21	317	1063	31.6	129.5
W_s (m s^{-1})	4.6×10^{-6}	5.5×10^{-5}	7.7×10^{-4}	6.6×10^{-3}	2.0×10^{-2}	4.1×10^{-2}	1.6×10^{-1}	1.1×10^{-4}	5.9×10^{-4}
ρ (kg m^{-3})	2650	2650	2650	2650	2650	2650	2650	1264	1097

Table 2[Click here to download Table: Table 2-Arrondi.doc](#)

Table 2. Annual sediment fluxes integrated between April 01, 1998 and March 31, 1999. Scenarios with Storms and /or Trawling resuspension include sediment input by rivers. Deposition rate for these scenarios excludes the deposited and exported sediment directly deriving from rivers. Once riverine sediment has been deposited on the shelf it is accounted in the resuspension, and subsequent deposition and export fluxes.

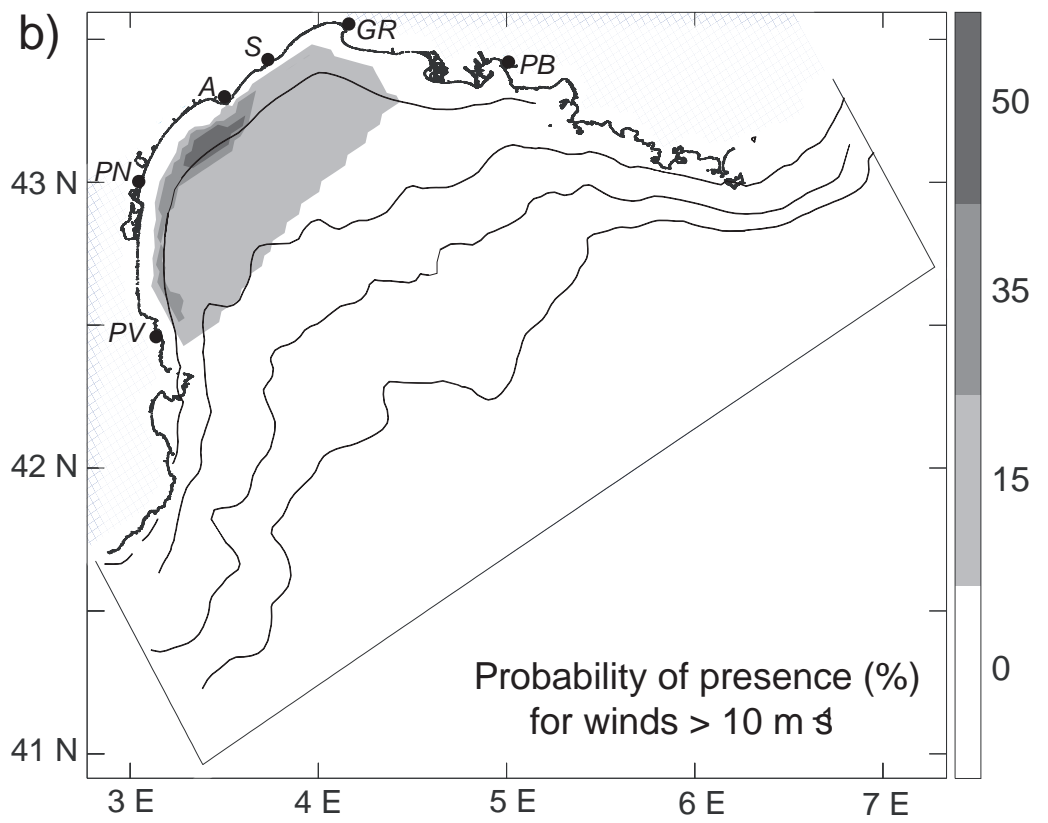
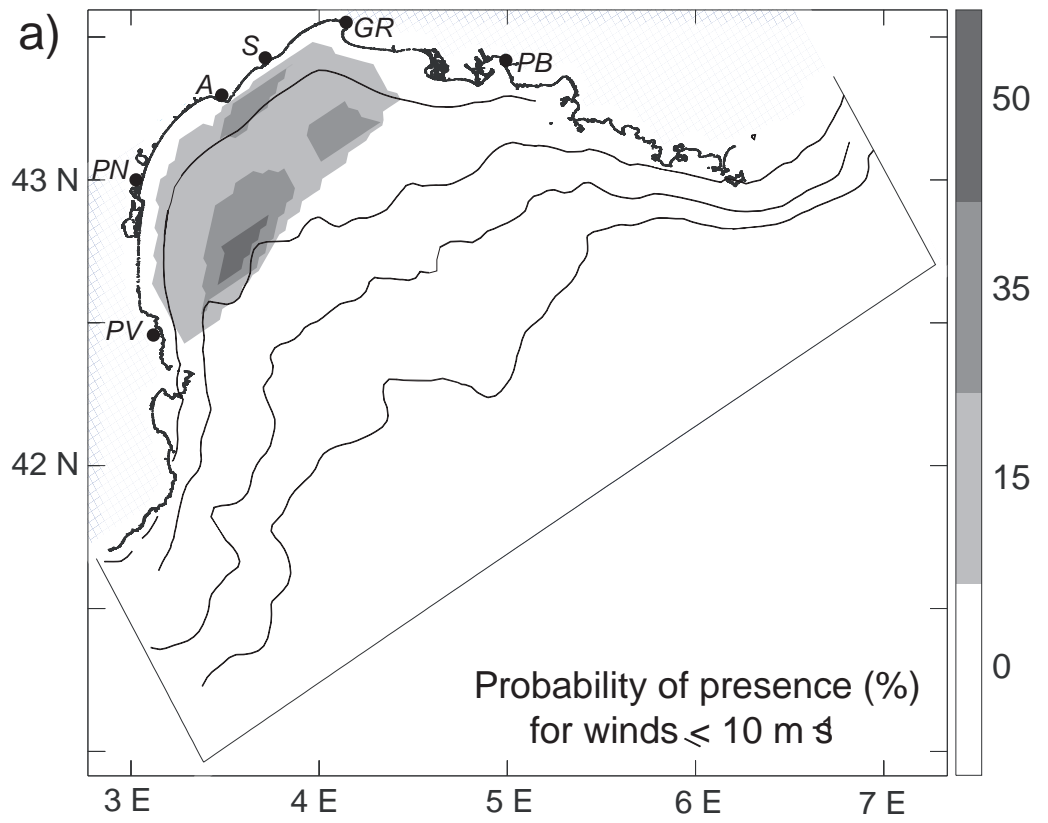
Scenario Sed Fluxes	Rivers	Storms	Trawling	Sum (Storms + Trawling)	Mixed (Storms and Trawling)
<i>River Discharge</i> (10 ⁶ T y ⁻¹)	3.6	3.6	3.6	3.6	3.6
<i>Shelf Erosion</i> (10 ⁶ T y ⁻¹)	0	35264.6	5.6	35270.2	35209.4
<i>Shelf Deposition</i> (10 ⁶ T y ⁻¹)	3.1	35255.4	5.2	35260.6	35200.1
<i>Shelf (Erosion- Deposition)</i> (10 ⁶ T y ⁻¹)	-3.1	9.2	0.4	9.6	9.3
<i>Shelf export</i> (10 ⁶ T y ⁻¹)	0.4	8.5	0.4	8.9	8.9

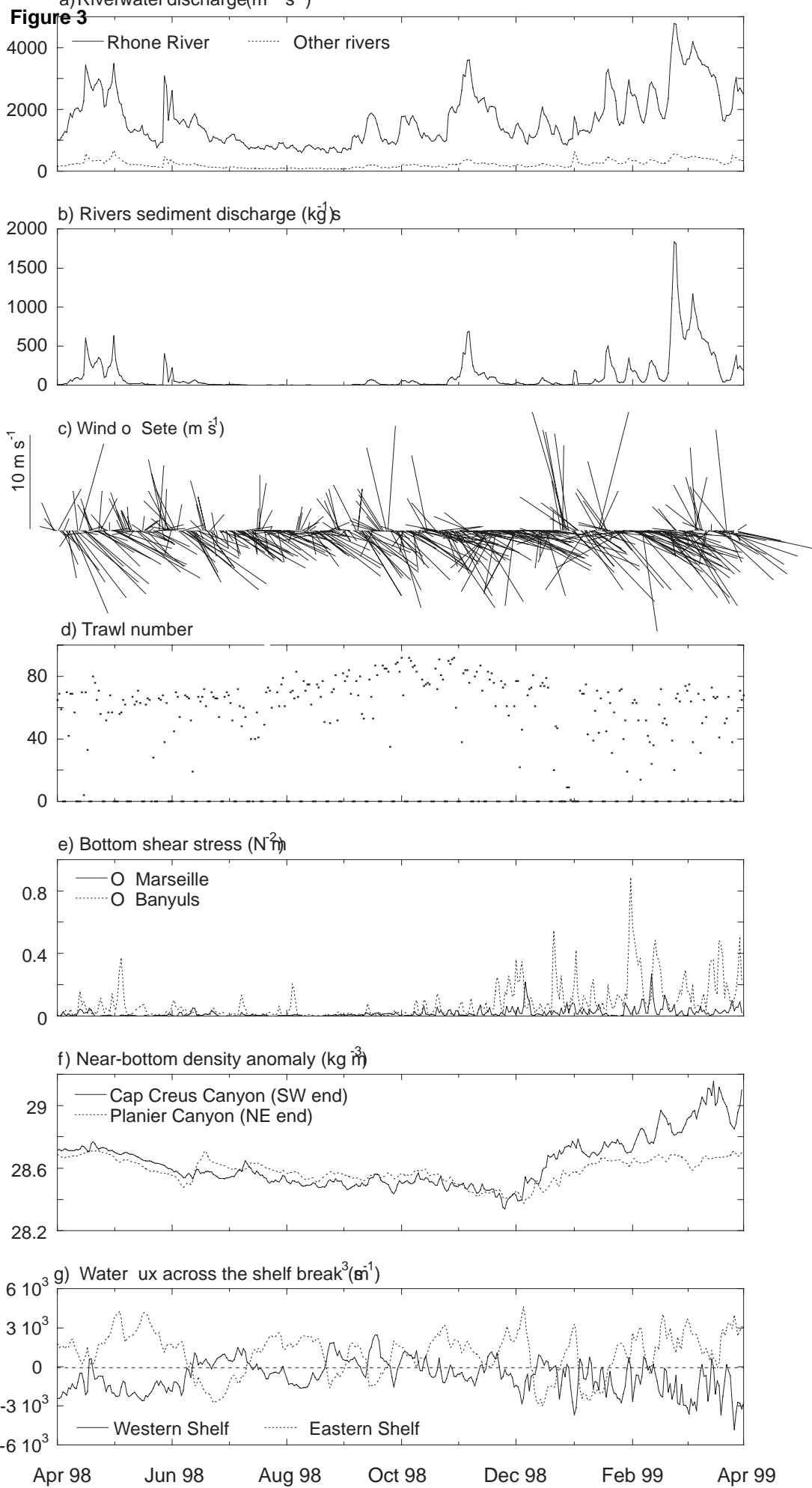
Figure 1



Ferre et al. Figure 1

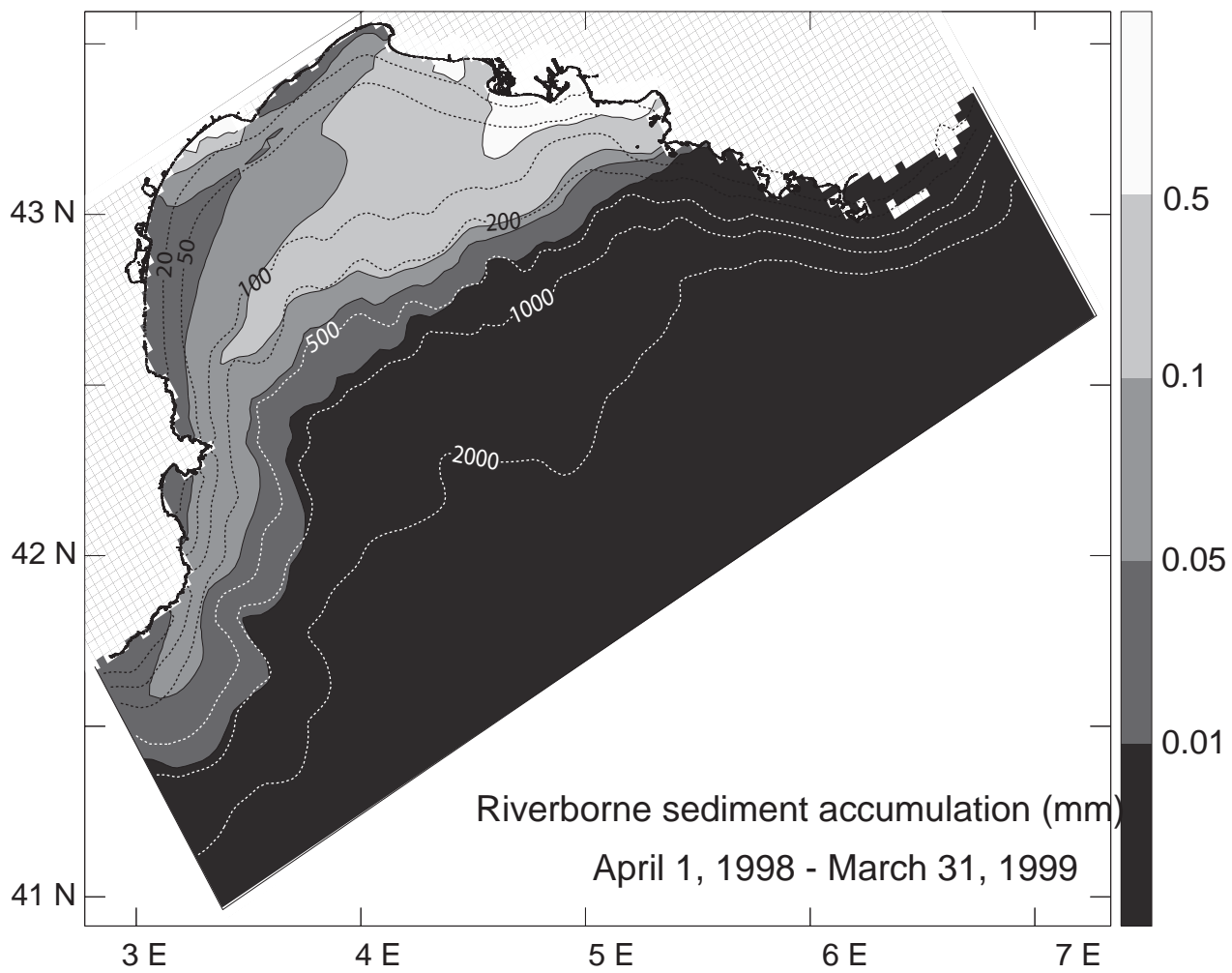
Figure 2





Ferre et al. Figure 3

Figure 4



Ferre et al. Figure 4

Figure 5

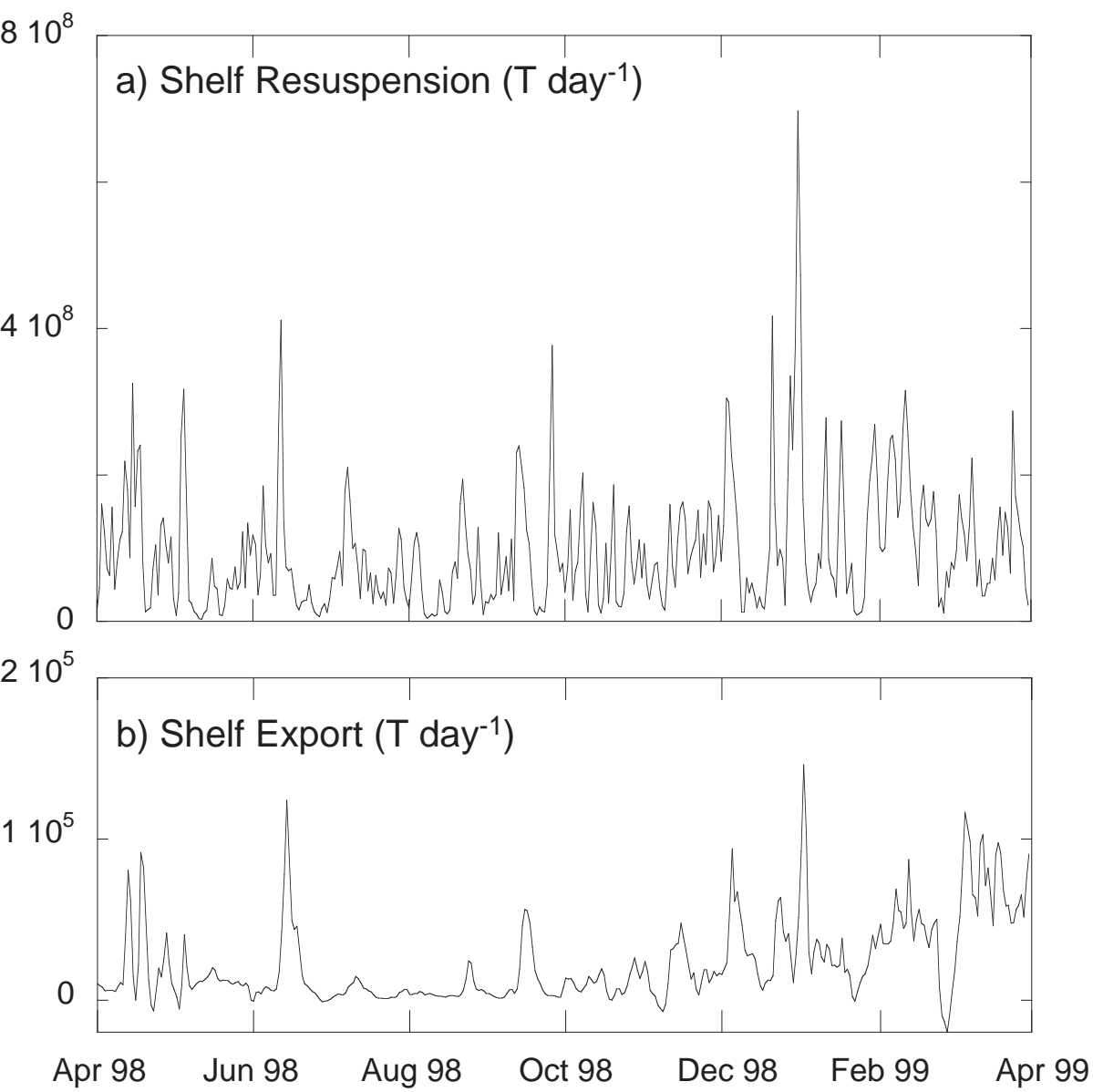
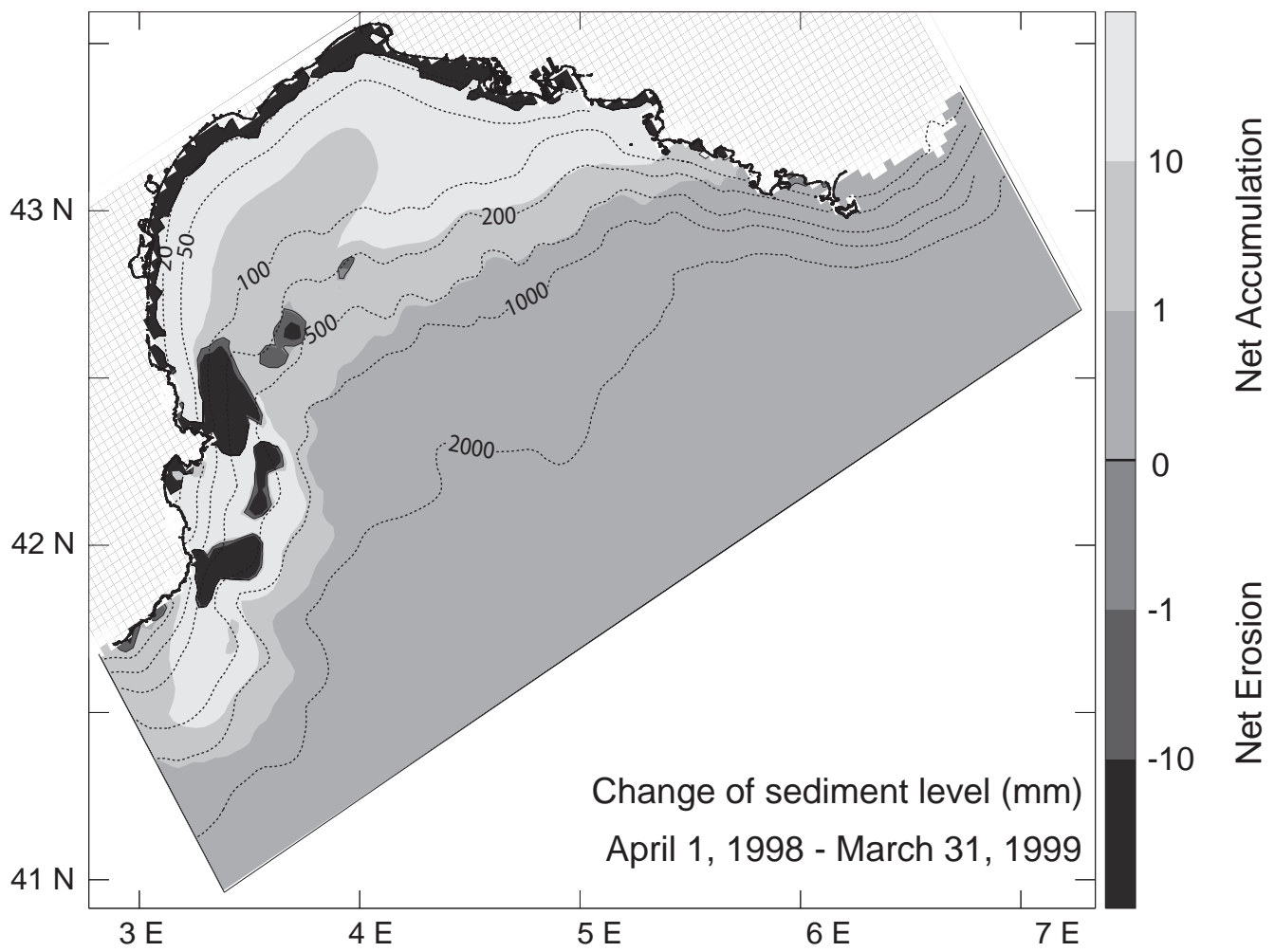
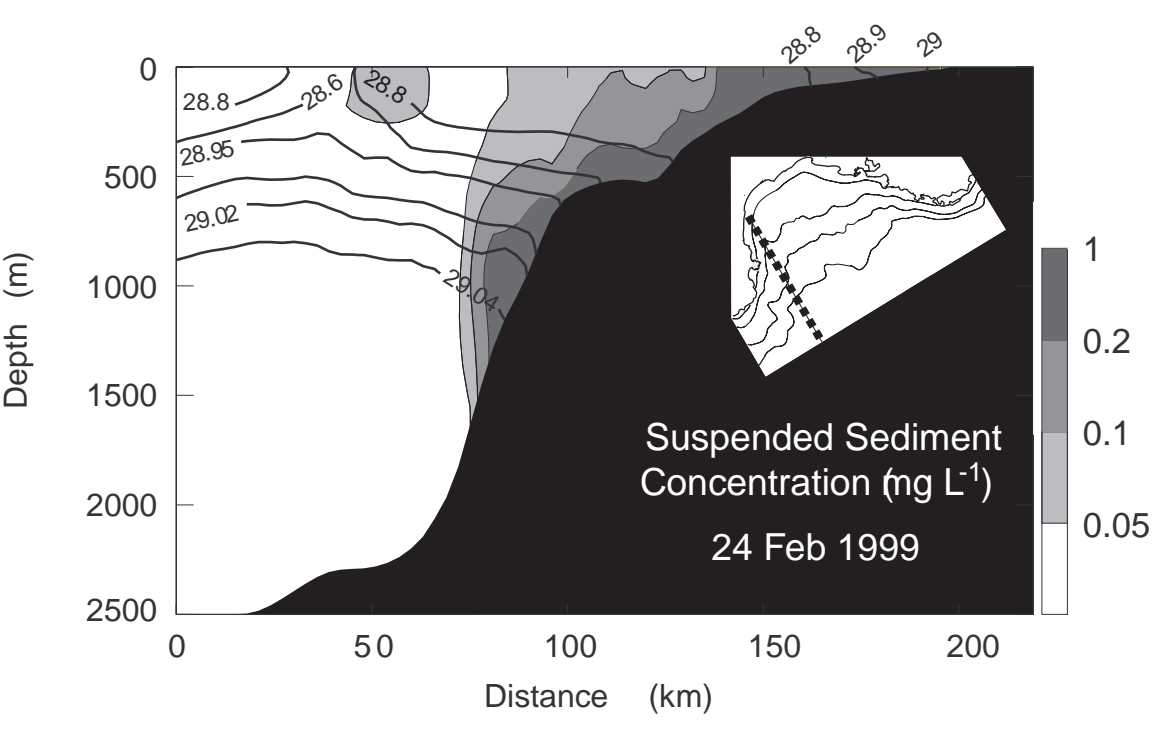
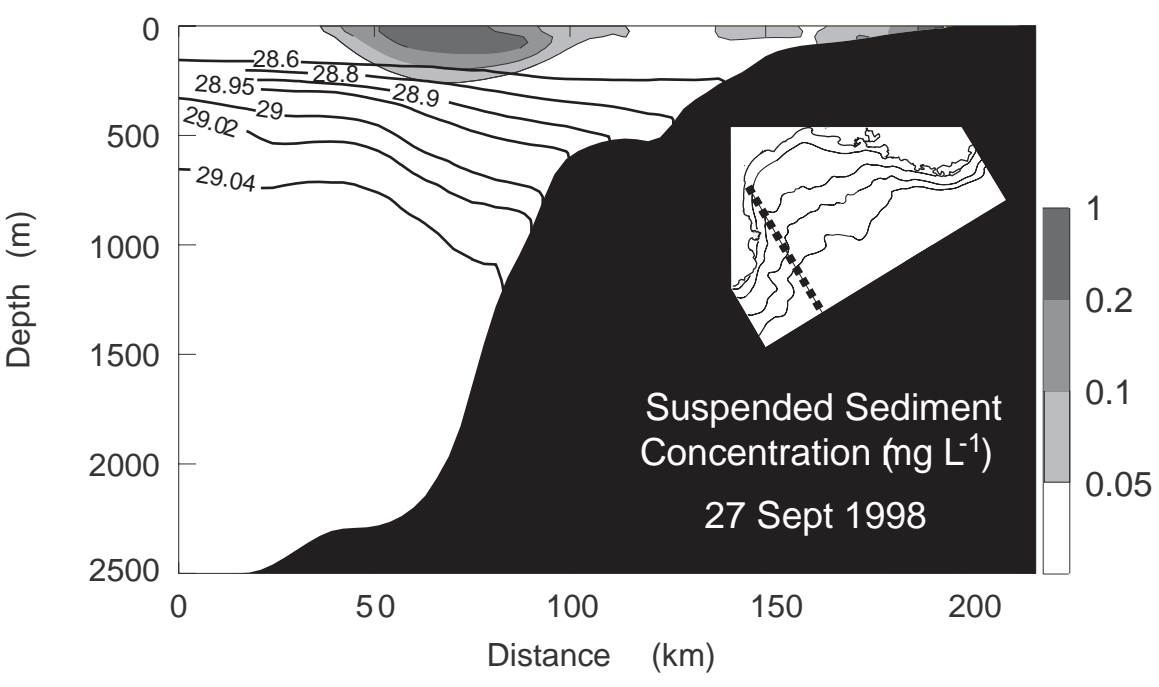


Figure 6



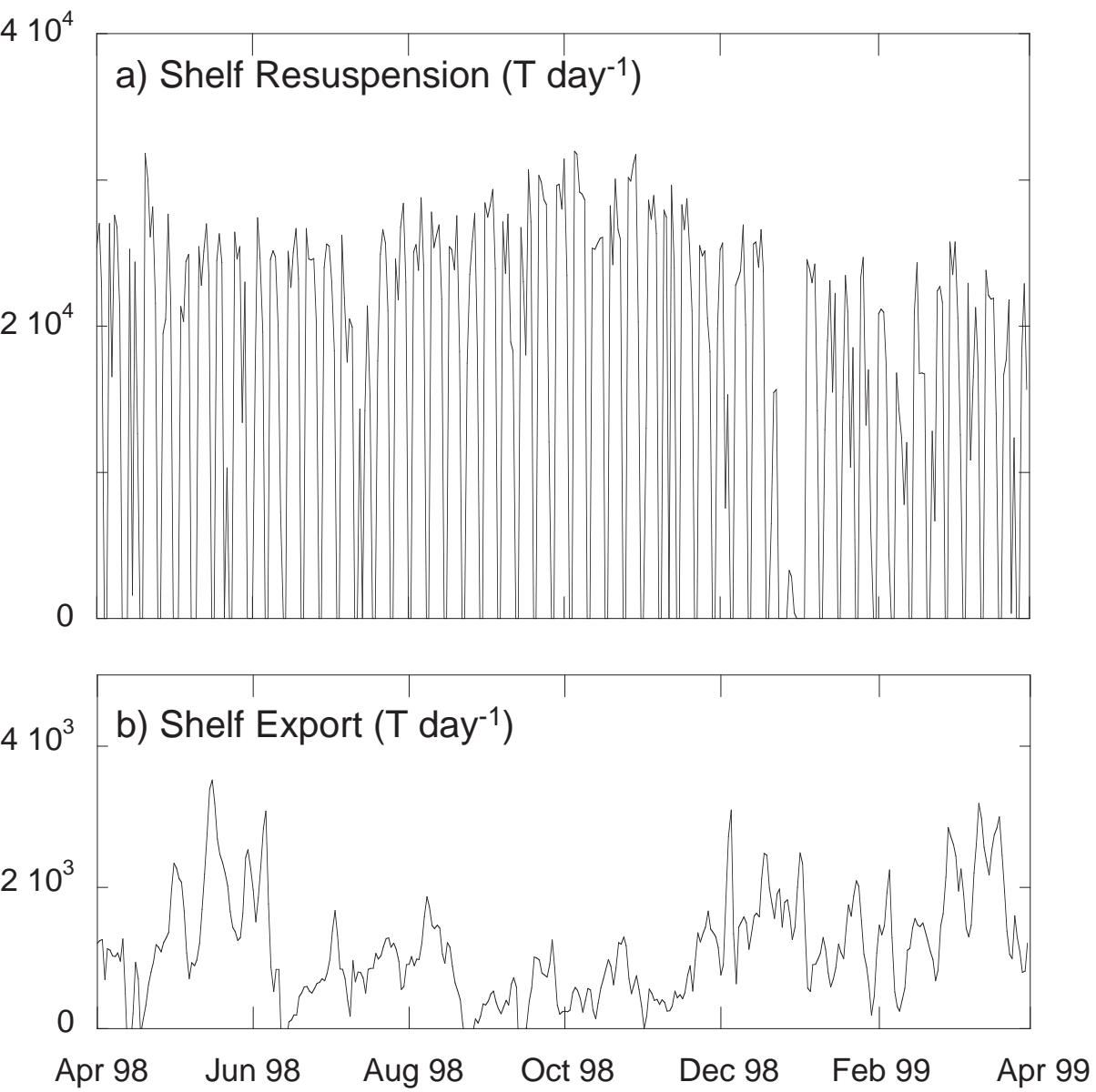
Ferre et al. Figure 6

Figure 7



Ferre et al. Figure 7

Figure 8



Ferre et al. Figure 8

Figure 9

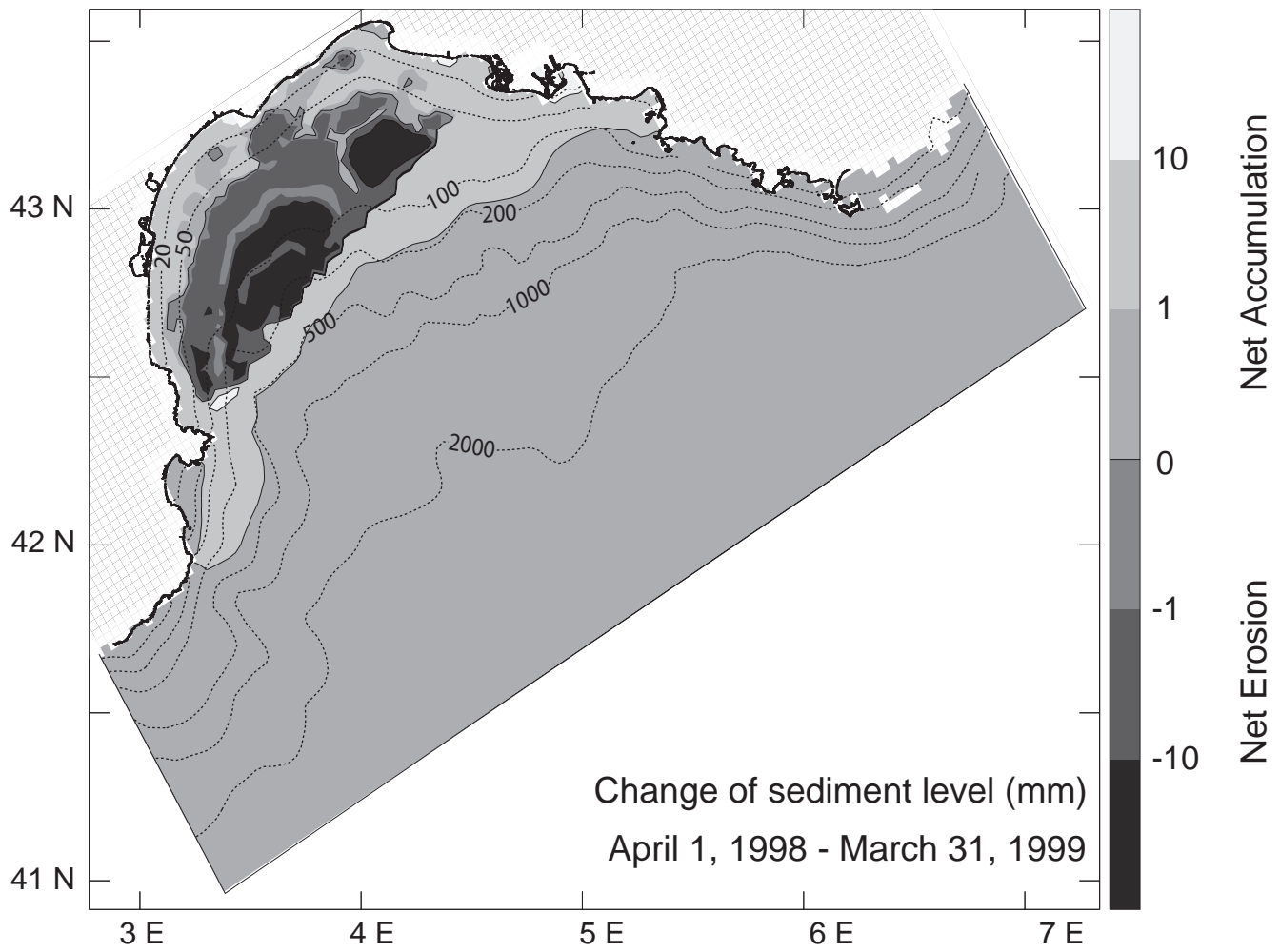
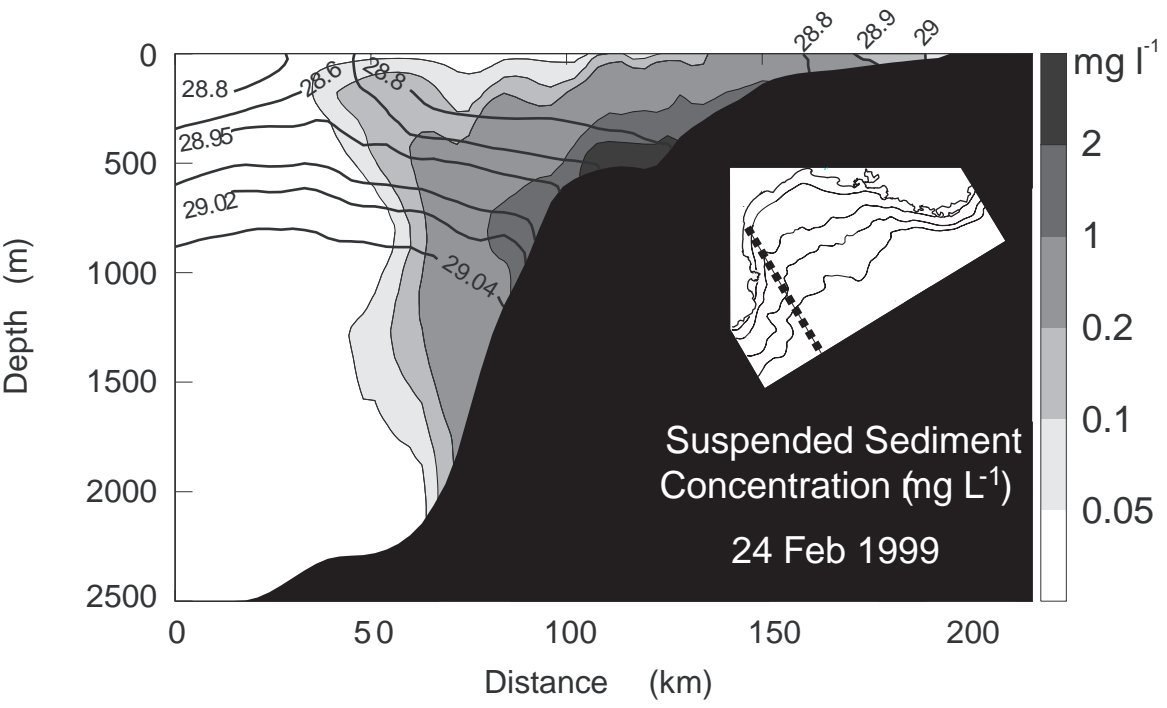
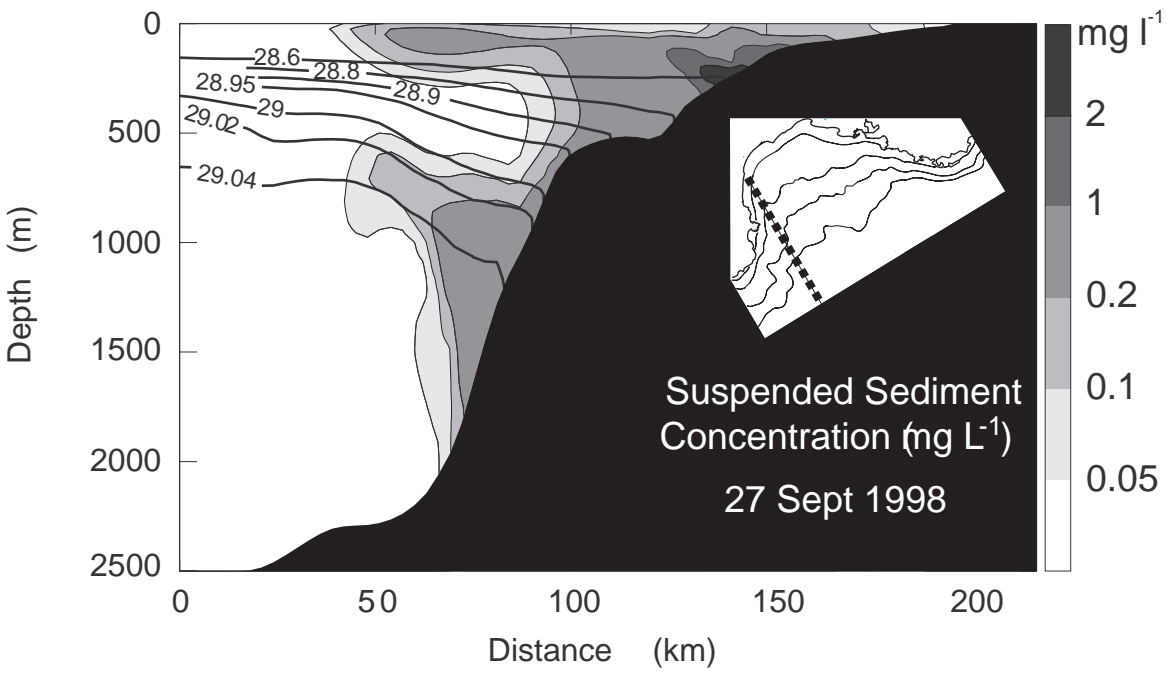


Figure 10



Ferre et al. Figure 10

Figure 11

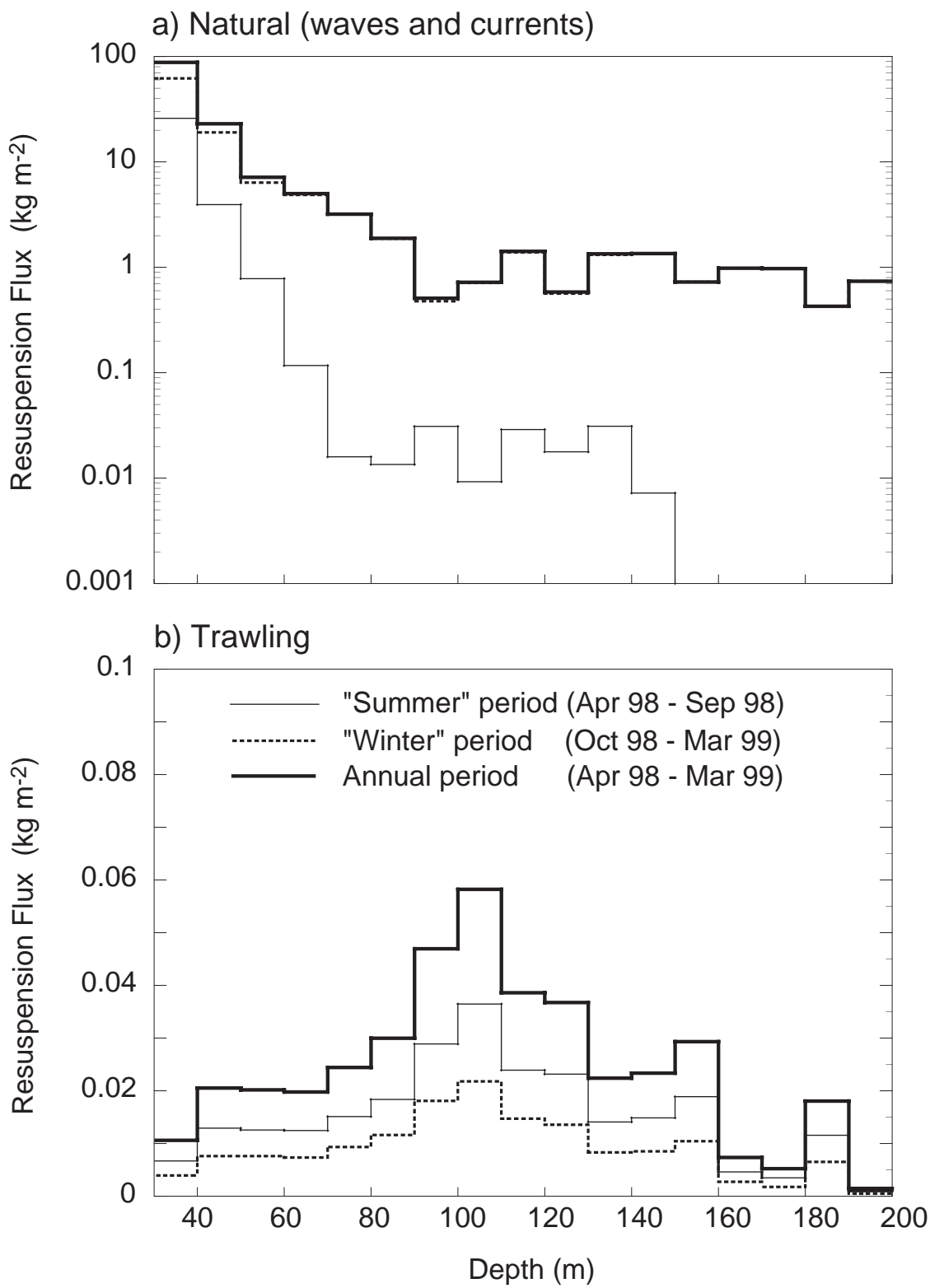
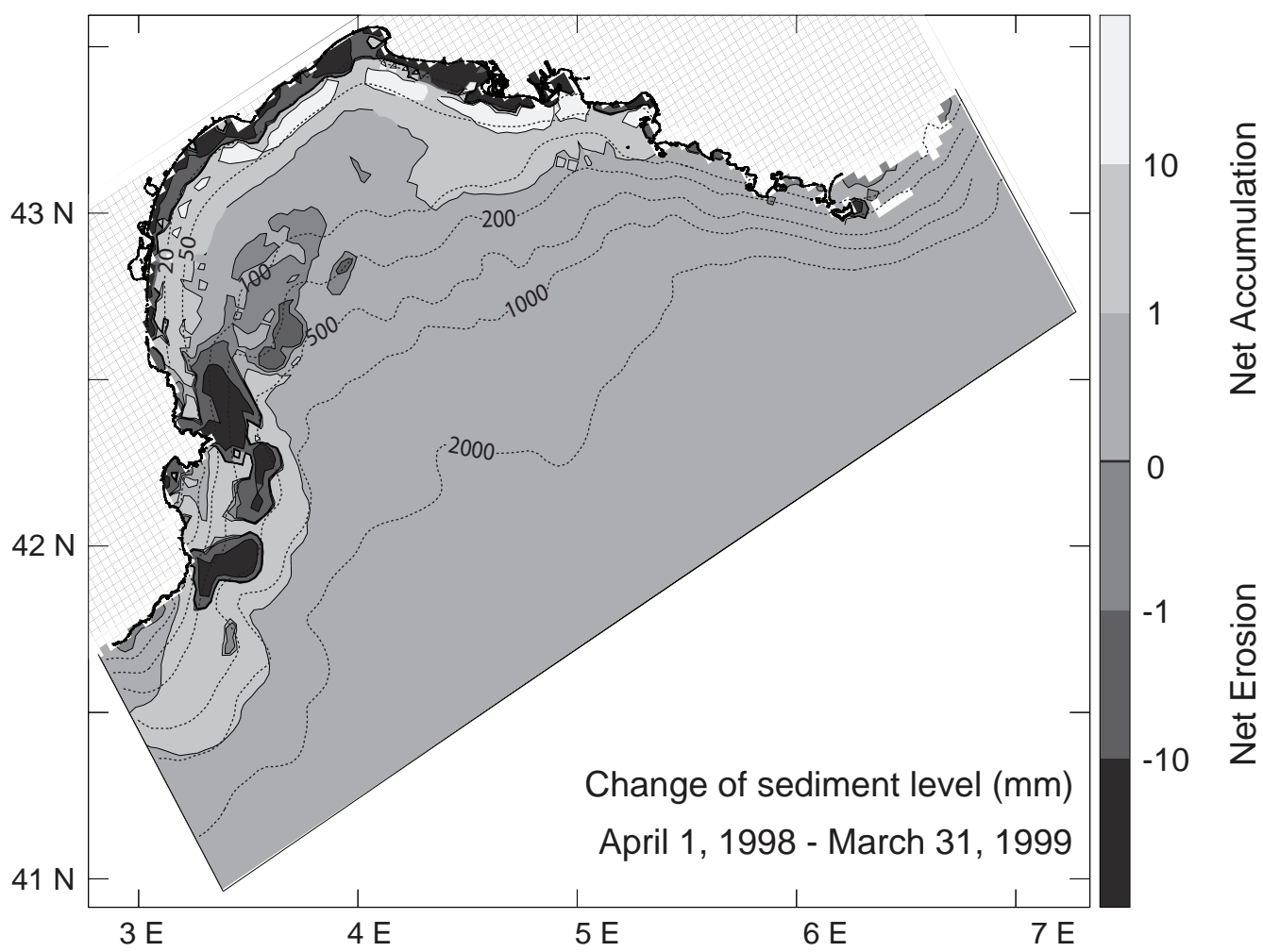
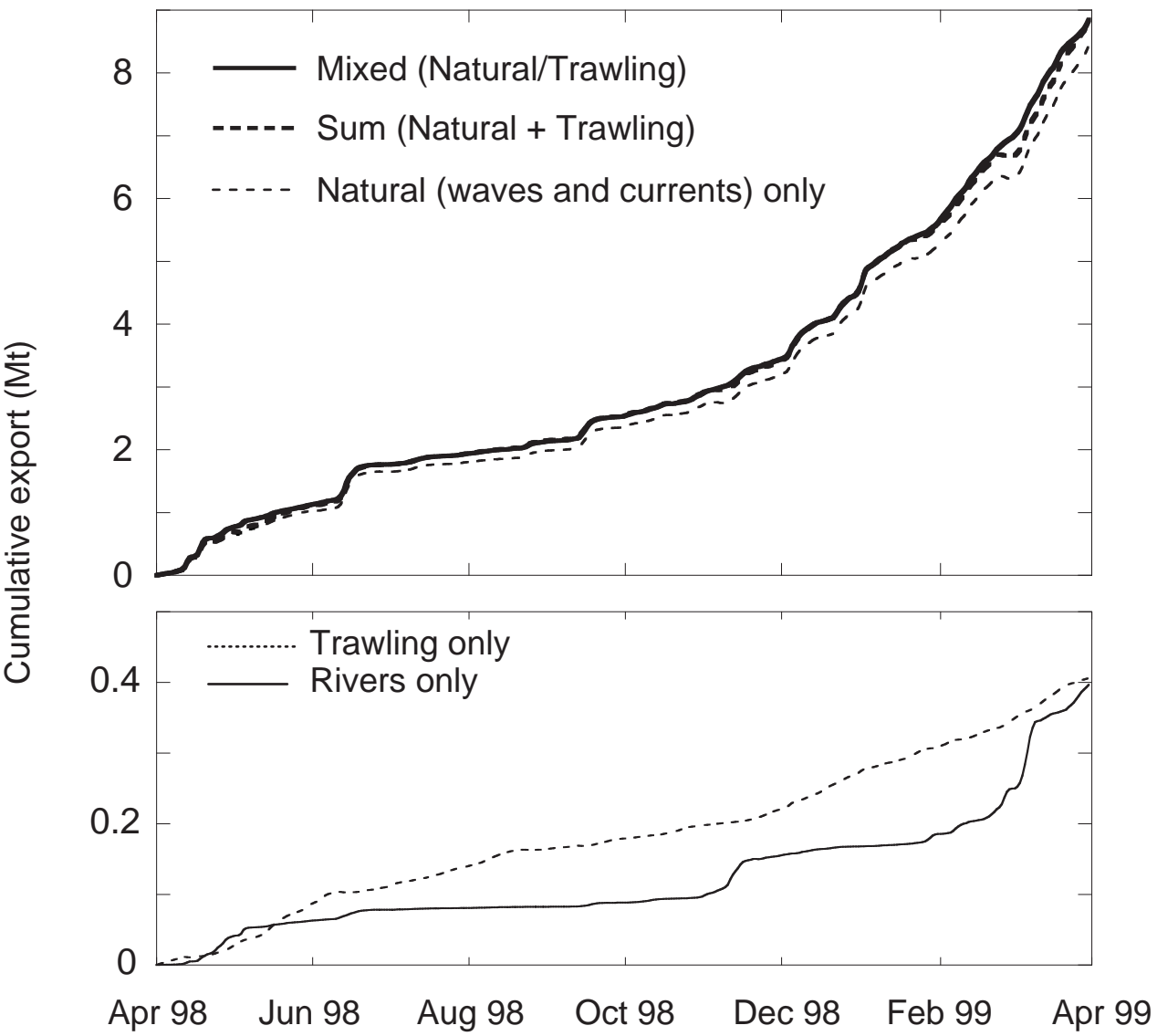


Figure 12



Ferre et al. Figure 12

Figure 13



Ferre et al. Figure 13